

Accretion in Evolved and Transitional Disks in Cep OB2: Looking for the Origin of the Inner Holes

Aurora Sicilia-Aguilar¹, Thomas Henning¹, Lee W. Hartmann²

sicilia@mpia.de

ABSTRACT

We present accretion rates for a large number of solar-type stars in the Cep OB2 region, based on U band observations. Our study comprises 95 members of the ~ 4 Myr-old cluster Tr 37 (including 20 “transition” objects; TO), as well as the only CTTS in the ~ 12 Myr-old cluster NGC 7160. The stars show different disk morphologies, with the majority of them having evolved and flattened disks. The typical accretion rates are about one order of magnitude lower than in regions aged 1-2 Myr, and we find no strong correlation between disk morphology and accretion rates. Although half of the TO are not accreting, the median accretion rates of normal CTTS and accreting “transition” disks are similar ($\sim 3 \times 10^{-9}$ and $2 \times 10^{-9} M_{\odot} \text{ yr}^{-1}$, respectively). Comparison with other regions suggests that the TO observed at different ages do not necessarily represent the same type of objects, which is consistent with the fact that the different processes that can lead to reduced IR excess/inner disk clearing (e.g., binarity, dust coagulation/settling, photoevaporation, giant planet formation) do not operate on the same timescales. Accreting TO in Tr 37 are probably suffering strong dust coagulation/settling. Regarding the equally large number of non-accreting TO in the region, other processes, like photoevaporation, the presence of stellar/substellar companions, and/or giant planet formation may account for their “transitional” SEDs and negligible accretion rates.

Subject headings: accretion disks — planetary systems: protoplanetary disks — stars: pre-main sequence

1. Introduction

In the last years, *Spitzer* observations have repeatedly shown that disk dissipation is a complex process, and that substantial evolution occurs to the dust grains and to the SED structure before the disk is rendered optically thin and disappears (e.g. van Boekel et al. 2003; Apai et al. 2005;

¹Max-Planck-Institut für Astronomie, Königstuhl 17, 69117 Heidelberg, Germany

²University of Michigan, 830 Dennison 500 Church St., Ann Arbor, MI 48109

Lada et al. 2006; Sicilia-Aguilar et al. 2006a, 2007, 2008b, 2009; Rodmann et al. 2006; Currie et al. 2009). By the age of 4 Myr, the typical spectral energy distribution (SED) shows that grain growth, dust settling, or both, have contributed to decrease the flaring of the disk and/or to lessen the dust opacity, resulting in lower luminosities in the near- and mid-IR compared to younger disks (Sicilia-Aguilar et al. 2006a). In some objects, the dust evolution has gone so far, that the disks seem to have been caught in the final act of dispersion, being in an intermediate stage between a normal, Class II object and a Class III source with an optically thin disk. Unlike the normal disks around classical T Tauri stars (CTTS), these “transition” objects (TO) show no significant near-IR excess, but retain optically thick disks at longer wavelengths, which suggest that they have inner opacity holes and are suffering inside-out clearing (Forrest et al. 2004; D’Alessio et al. 2005; McCabe et al. 2006; Sicilia-Aguilar et al. 2006a). How the dusty disk dissipates, and whether all disks go through the TO phase before disappearing, remains uncertain. Regions in the 1-10 Myr age range are found to contain TO, although they seem to be more common in older clusters (Sicilia-Aguilar et al. 2006a, 2009; Currie et al. 2009). The fact that at any age we find objects with and without disks, and the abundance of flattened disks (optically thick, geometrically thin) in clusters of intermediate age (Sicilia-Aguilar et al. 2006a; Currie et al. 2009) suggest a variety of physical processes leading to disk dissipation.

In addition to dust, the disk contains about 99% of gas, which controls the dust dynamics, at least until self-gravitating clumps have formed (Schräpler & Henning 2004; Johansen & Klahr 2005; Johansen et al. 2007). The decrease in disk fraction over time is accompanied by a “parallel” decrease in accretion activity and in the magnitude of the accretion rates (Hartmann et al. 1998; Sicilia-Aguilar et al. 2006b; Fedele et al. 2009). Nevertheless, detecting the gas in the inner few-AU where planet formation is thought to occur, is complicated. Near-IR spectroscopy has revealed the presence (or lack) of gas in the innermost disk of some T Tauri stars with different disk morphologies (Najita et al. 1996, 2003; Carr et al. 2001; Rettig et al. 2005; Pascucci et al. 2006, 2009; Goto et al. 2006; Carmona et al. 2007, 2008; Salyk et al. 2009), but the procedure is too expensive to include large, statistically significant samples of disks. Detecting the gas as it falls onto the star via chromospheric accretion (Königl et al. 1991) is an easier procedure to constrain the presence of gas in the innermost disk for large number of objects.

Objects that have partially dispersed/coagulated their disks (TO) are especially important to understand the factors involved in disk evolution. While there is no consensus about the definition and characteristics of TO, we here follow the rule of considering TO those objects that show zero or negligible IR excess at $\lambda < 6\mu\text{m}$ and normal IR excess (CTTS-like) at longer wavelengths, compared to the photospheric emission. According to our definition, TO have reduced IR colors with $[3.6]-[4.5] < 0.2$ mag and a sharp increase in the excesses usually around $8\mu\text{m}$ (Sicilia-Aguilar et al. 2006a). A similar definition has been used by Muzerolle et al. (2009). For solar-type (late G-early M¹) stars, this suggests the presence of an inner hole or a highly evolved/settled and

¹A $1M_{\odot}$ star aged ~ 1 Myr has an spectral type $\sim K6$ (Siess et al. 2001).

probably optically thin inner disk with radius of a few AU within a disk that is flared and optically thick at larger distances from the star (D’Alessio et al. 2005), consistent with inside-out clearing of the disk (Hayashi et al. 1985). The presence of accretion and the accretion rates are necessary parameters to distinguish between the different scenarios that create the inner holes of the TO (photoevaporation, dust coagulation, planetesimal formation, formation of giant planets). Systems empirically classified as TO do not form a uniform class of objects, but include binaries (Ireland & Kraus 2008), objects with giant planets (Setiawan et al. 2008), and cases where strong dust coagulation and/or photoevaporation have produced an optically thin disk (Pascucci & Sterzik 2009). Since these different processes operate on different timescales, it is not evident that the bulk of TO in regions with different ages should be dominated by the same type of objects (Alexander & Armitage 2009).

Here we present the results of a deep U band survey of the young clusters Tr 37 and NGC 7160, both part of the Cep OB2 region. Section 2 describes the observations, data reduction, and the calculation of the accretion rates. In Section 3 we analyze the potential correlations of \dot{M} with disk structure, age, and stellar mass, and explore the fraction of stars that display variable accretion rates. Finally, we summarize our conclusions in Section 4.

2. Observations, data reduction, and accretion rates

2.1. The Cep OB2 region: previous observations

Cep OB2 is a bubble-shaped star-forming region (Patel et al. 1998) located at 900 pc distance (Contreras et al. 2002). It contains several OB stars and the young clusters NGC 7160 (median age ~ 10 -12 Myr) and Tr 37 (median age ~ 4 Myr). Tr 37 and NGC 7160 contain a significant population of solar-type stars (~ 180 and ~ 60 late G-M2-type members, respectively). A younger population (aged ~ 1 Myr) is located to the west of Tr 37 (Sicilia-Aguilar et al. 2005b, 2006a). Optical spectroscopy was used to determine the membership, spectral types, and the presence of accretion. The clusters have also been observed with *Spitzer* IRAC ($\lambda=3.6$ -8.0 μm) and MIPS ($\lambda=24$ and 70 μm ; Sicilia-Aguilar et al. 2006a). In Tr 37, the disk fraction for solar-type stars is $\sim 45\%$, and more than 95% of the disks show low IRAC fluxes (compared to Taurus), which suggests dust evolution (grain growth/settling), especially strong in the innermost disk. About 10% of the objects are TO. In NGC 7160, only two of the known 60 solar-type members conserve their disks. The accretion rates of 45 members of Tr 37 had been estimated via U band photometry (Sicilia-Aguilar et al. 2005b). UVRI observations were obtained with the 1.2m telescope at the the Fred Lawrence Whipple Observatory (FLWO), but the VRI and U band data were not taken simultaneously, and the survey was complete only down to few times $10^{-9} M_{\odot} \text{ yr}^{-1}$. High-resolution H α spectroscopy of the Tr 37 members (Sicilia-Aguilar et al. 2006b) revealed many more accreting objects, suggesting that deeper U band observations were necessary to fully study the dependence of accretion on disk structure, age, and stellar mass.

2.2. Observations and data reduction

The U V R_J I_J observations of Tr 37 were obtained in service mode during 3 nights in 2007 June 9-11, using the wide field camera LAICA mounted on the 3.5 m telescope in Calar Alto, Spain. LAICA is a 2×2 mosaic of 4 CCDs (which we name a,b,c,d), each covering a $15.3' \times 15.3'$ field of view with a large gap ($15.3' \times 15.3'$) in between. We obtained four pointings in Tr 37 (named 1,2,3,4 in the Table 1), in order to cover a large field (approximately $45' \times 45'$, containing most of the Tr 37 members) and to avoid the brightest stars in the cluster. The exposure time was 3×120 s in U, and for V R_J I_J , we obtained short and long exposures 3×10 s and 3×60 s, respectively. The 3 dithered exposures ensure a good removal of cosmic rays, minimize CCD defects, and provide a large dynamical range, complete in the magnitude ranges $U \sim 15-21$, $V \sim 13-21$, $R_J \sim 12-21$, and $I_J \sim 11-20$ (from now on, R_J and I_J are simply written R and I). The time span of the observations was less than 1.5 h for the objects observed in the same night. Pointing 1 (UVRI) was observed during the first night. During the second night, we observed the pointing 2 (UVRI) and U band for the pointing 3. During the third night, we obtained VRI for the pointing 3, and UVRI for the pointing 4. Therefore, all the UVRI observations for the pointings 1,2, and 4 can be considered nearly-simultaneous, and the U band observations of pointing 3 are separated by ~ 23 h from the pointing 3 VRI (see Table 1). All the nights were photometric, with seeing in the range 0.6-1.3".

The observations of NGC 7160 were obtained in 2007 October 5, using the 70 cm King telescope of the Max-Planck-Institut für Astronomie at the Königstuhl, Heidelberg, Germany. The telescope is equipped with a CCD with a field of view $\sim 18' \times 18'$ and standard UBVR $_J$ I_J filters. We followed a similar strategy, obtaining 3 exposures of 10s and 240s in U, and 3×120 s for the rest of filters, in a field centered on the cluster, which includes the only two low-mass sources with disks detected with *Spitzer* in NGC 7160 (only one of them was detected in U). Given the smaller diameter of this telescope, the survey is complete down to $U \sim 18$, $V \sim 18$, $R \sim 17.5$, $I \sim 17$ only. The night was clear but not photometric, and the seeing was poor (2").

The data from the two telescopes were reduced following standard procedures with IRAF² within the *noao.imred.ccdred* package to do the bias and flat field corrections, and *noao.digiphot.apphot* for aperture photometry. The flux calibration was obtained as relative (or differential) photometry (Herbst et al. 2000; Briceño et al. 2001), which we have also used to calibrate the variable star GM Cep (Sicilia-Aguilar et al. 2008a). For each field and band, we matched our instrumental photometry to existing calibrated data. The fact that most stars in the fields are non-variable allows us to derive the calibration zeropoints for our data. The UVRI data for Tr 37 and the VRI data for NGC 7160 were compared with our previous optical data from the Fred Lawrence Whipple Observatory (Sicilia-Aguilar et al. 2005b), properly transformed from the Cousins FLWO filters into the standard Johnsons system (Fernie 1983). Lacking U data for NGC 7160 from our FLWO catalog, the U band observations of NGC 7160 were calibrated comparing with the catalog from

²IRAF is distributed by the National Optical Astronomy Observatories, which are operated by the Association of Universities for Research in Astronomy, Inc., under cooperative agreement with the National Science Foundation.

De Graeve (1983). Since the calibration involves a large number of stars observed simultaneously in the same CCD, the zeropoint uncertainties are typically lower than 1%, so the magnitude errors are dominated by the signal to noise ratio (S/N). The magnitudes and their errors are listed in Table 2. To ensure the quality of the photometry, all images were visually inspected to remove all objects that could be affected by nearby stars, scattered light from bright sources, or CCD artifacts. We also compared the photometry from our previous studies (Sicilia-Aguilar et al. 2004, 2005b) and those stars displaying magnitude variations $\Delta V \geq 0.5$ mag are labeled as “variables” in Table 2. Note that $\sim 65\%$ (62/96) of the objects display small magnitude variations (≥ 0.1 mag; see Section 3.4).

2.3. Accretion rates

The accretion rates were derived from U broad band photometry following the correlation between accretion luminosity (L_{acc}) and U band excess luminosity (L_U) found by Gullbring et al. (1998):

$$\log(L_{acc}/L_{\odot}) = 1.09 \log(L_U/L_{\odot}) + 0.98 \quad (1)$$

The accretion luminosity corresponds to the energy released by the matter falling onto the star. The accretion rate can be obtained from the accretion luminosity if the stellar mass and radius (M_* , R_*) are known, assuming that the accreted matter reaches the star in free fall via chromospheric accretion from a distance $R_{in} \sim 5 R_*$:

$$L_{acc} \sim GM_*\dot{M}/R_*(1 - R_*/R_{in}) \quad (2)$$

To calculate the excess of luminosity in U band (L_U) for a given object, we need to know the measured U band luminosity and the expected U band luminosity for a star with the same spectral type and luminosity. A good extinction correction and accurate spectral type are essential. The spectral types for the Tr 37 and NGC 7160 members were derived from low-resolution spectroscopy in Sicilia-Aguilar et al. (2004) and Sicilia-Aguilar et al. (2005b), and are accurate up to 1 subtype (for K and M stars) and 2 subtypes (for G-type stars). We calculated the extinction from the V-R and V-I colors, applying the relations in $E(V-R)=0.249 A_V$ and $E(V-I)=0.521 A_V$ (Cardelli et al. 1989) and considering the standard colors for each spectral type (Kenyon & Hartmann 1995). Circumstellar matter may produce a non-standard extinction law, but the similar A_V values obtained from V-R and V-I suggest that the main source of extinction towards Cep OB2 is standard interstellar matter. Due to pointing offsets, a few sources lack V photometry, so we derived their extinction from $E(R-I)=0.272 A_V$. Finally, for the objects for which only one band (V, R, or I) was available, we consider previous measurements of the extinction (Sicilia-Aguilar et al. 2004, 2005b) with an error of 0.45 mag (corresponding to the standard deviation of A_V in the cluster). If A_V has

not been measured previously, we take it to be the average of the cluster with its standard deviation ($A_V=1.67\pm 0.45$ mag; Sicilia-Aguilar et al. 2005b). The final uncertainties in the extinction reflect the errors in the photometry, spectral type, and the variations between A_V calculated via $E(V-R)$ and $E(V-I)$.

The U band luminosity is derived from the U magnitude corrected by the extinction. The U band luminosity due to the stellar photosphere is calculated using the U-V and V-I colors and the bolometric correction for standard stars (Kenyon & Hartmann 1995), together with the extinction-corrected I magnitude (or, in objects without I magnitude, R or V). Magnitudes are transformed into luminosities taking into account the zero point flux and bandwidth for U band (4.19×10^{-9} erg s $^{-1}$ cm $^{-2}$ Å $^{-1}$ and 680 Å, respectively). The stellar masses (M_*) and ages are calculated from the extinction-corrected V vs. V-I diagram and the Siess et al. (2000) isochrones, and the stellar radii (R_*) are obtained from the total stellar luminosities and the effective temperatures. In the few cases where no V or no I are available, we use the total photospheric luminosity and effective temperature on a HR diagram and the Siess et al. (2000) isochrones to derive the stellar parameters. Knowing M_* , R_* and the excess U band luminosity L_U , the accretion luminosity and accretion rate are derived from Equations 1 and 2. The results are listed in Table 3.

Given the number of parameters involved in the mass accretion calculation, it is important to assess if the measured \dot{M} is significant. Since the quantities required for the calculation of \dot{M} are not independent (in particular, the two main contributors to the uncertainty, the spectral type and the extinction, are strongly correlated), standard error propagation largely overestimates the errors. Moreover, the relation between the U magnitude and L_U is highly non-linear, so the errors are asymmetric in the positive and negative directions. We therefore estimated the errors generating 5000 sets of artificial data per object. The artificial data were constructed by adding Gaussian noise with an amplitude corresponding to the measured errors to the involved parameters. We then consistently derived A_V and repeated the calculation of \dot{M} for each one of the 5000 sets. The errors for each star are derived from the \dot{M} distribution as the standard deviation in the positive and negative directions. We consider an accretion rate to be safely detected (>0.99 probability) if L_U is positive in more than 99% of the simulations. If not, we estimate a $3\text{-}\sigma$ upper limit to \dot{M} , except for those objects for which $H\alpha$ observations have ruled out the presence of accretion, especially if our *Spitzer* data reveal no excess emission, given that $H\alpha$ is a more sensitive criterion for low accretion rates than L_U . For these narrow- $H\alpha$ objects, we consider the accretion rate to be $<10^{-11} M_\odot \text{ yr}^{-1}$, which is in agreement with the line profile fitting for M-type stars (Muzerolle et al. 2003) and with the observations of late-K objects in the η Cha cluster (Lawson et al. 2004)³. For simplicity, these “non-accreting” objects are labeled with $\dot{M}=0 M_\odot \text{ yr}^{-1}$ in Table 3.

In addition, there are other sources of error: uncertainties in the stellar radius, stellar mass, and size of the stellar chromosphere. These uncertainties do not change the detectability of the accretion rate, but vary \dot{M} by a typically small multiplicative factor (2-3; Gullbring et al. 1998).

³ Note that the limit will be lower for M-type objects and higher for the early K and G stars.

Since the accretion rates are found to vary by a factor of few when the same star is measured over time, these uncertainties do not affect our conclusions. The ability to detect accretion via U band excess emission also depends on the spectral type, which in our sample varies between G8 and M2.5 (median spectral type K7). For M stars, which have small intrinsic U band photospheric luminosity, small accretion rates result in detectable U band excess. For early K and G stars, a contrast problem appears as the U photospheric luminosity is much stronger than the L_U caused by relatively large accretion rates (10^{-8} - 10^{-9} M_{\odot} yr^{-1}). Therefore, some of our \dot{M} measurements for the most massive stars are only (high) upper limits. This has to be taken into account as a source of bias when studying the relation between the stellar mass and the accretion rate. For the typical late K-early M star in our sample, our U band photometry is sensitive to accretion rates of the order of $\sim 10^{-10}$ M_{\odot} yr^{-1} .

Comparing with our previous results, in particular, with the $H\alpha$ high-resolution spectroscopy with Hectochelle (Sicilia-Aguilar et al. 2006b), we find a very good agreement. All the objects with broad $H\alpha$ are found to be accreting or have upper limits consistent with the typical accretion rates found in other cluster members. We found an inconsistency between the spectral types in Sicilia-Aguilar et al. (2005b) and the VRI colors of two G-type stars, 12-1091 and 11-581. They appeared to be too red and had U magnitudes below the photospheric level, even assuming the large extinctions derived from VRI. Considering that our spectral types were more uncertain for G-type stars, we checked our spectra (taken with FAST and Hectospec; Sicilia-Aguilar et al. 2005b) comparing them to new standard stars and similar cluster members. The new spectral types (K2 for 12-1091 instead of G2.5; G9 for 11-581 instead of G5) are fully consistent with the photometry, and produce a more reliable value of A_V (with a similar value when derived from E(V-I) and E(V-R)). Two objects are inconsistent in the sense that they lack evidence of a disk and have narrow $H\alpha$ profiles, but display U band excess (12-1984 and 12-1422). They both have non-simultaneous observations (pointing 3c), which may explain the disagreement. The star 12-1422 is nevertheless a special case, since it does not display any detectable IR excess nor $H\alpha$ broadening, but had a high $H\alpha$ EW (-17 \AA for a M0 star) measured with our low-resolution spectra. Although its accretion rate is close to our detection limit, we might consider it as a potential accreting TO with a large inner hole, to be confirmed with future observations. Accretion in objects with no excess at $8\mu\text{m}$ seems rare, although here we confirm the case of 13-819, which had been previously detected to have broad $H\alpha$ despite the lack of excess at all IRAC wavelengths.

Finally, two TO with narrow $H\alpha$ appear now to be accreting (12-1009 and 72-875), and two more have upper limits consistent with accretion (14-197 and 12-595). For 12-1009, the data are non-simultaneous, and the star is known to have strong variability. The star 72-875, which is probably a single-lined spectroscopic binary (SB1) and has strong MIPS excess but narrow $H\alpha$, is now found to have a U band excess. IRS spectroscopy (Sicilia-Aguilar et al. in prep.) reveals that it is a TO with no excess at wavelengths shorter than $\sim 7\mu\text{m}$, so the object seems to have suffered a large increase in its accretion rate within a few years (see Section 3.4). The TO 14-197 is a similar mass spectroscopic binary, and we thus believe it is most likely non-accreting. The star

12-595 shows anomalous colors and extinction, being probably affected by scattering, non-standard extinction, and/or strong variability. Its U and VRI magnitudes are non-simultaneous and its LAICA V magnitude differ from the FLWO values by 1 magnitude, which suggests that the object is strongly affected by variable extinction by circumstellar material. Although they are a minority, all the inconsistent or potentially inconsistent objects are excluded from the analysis and discussion below.

As an additional note, here we confirm once more (as stated in Sicilia-Aguilar et al. 2006b) that even detailed criteria to distinguish accreting and non-accreting stars based on H α equivalent width (EW) alone (e.g., White & Basri 2003) may misclassify a certain number of objects with low accretion rates or active WTTS. This is in general not important for statistical purposes, especially in young clusters with typically high accretion rates. Nevertheless, it may become a problem in older regions like Tr 37 and NGC 7160 where low \dot{M} is the rule. In our study, the White & Basri (2003) criterion for H α EW would misclassify 7 objects out of 96 (11-1209, 11-581, 12-1091, 13-819, 13-1048, 13-1250, 22-1418, see Table 3). Therefore, other observations (especially high-resolution H α spectroscopy) are important to constrain the presence of accretion in the objects with the lowest rates.

3. Analysis

3.1. Gas accretion and dust evolution

In order to check the relation between accretion rates and dust evolution, we compare the disk morphology with the measured \dot{M} . It is not easy to define a tracer of disk morphology or SED slope in the Cep OB2 members, given that the typical SED slope varies between the near- and mid-IR, with most objects showing a “kink” or slope change around 6-8 μm (Sicilia-Aguilar et al. 2006a). Therefore, we measure the SED slope (α) at different wavelengths, and compare the α values with the measured accretion rates (Figure 1). According to our empirical definition, TO have SED slopes consistent with photospheres at $\lambda < 6\mu\text{m}$, together with negligible excess emission ($[3.6]-[4.5] < 0.2$ mag) down to this wavelength. In our Spitzer study, we did not include as TO objects having only a weak excess at 8 μm (named as “e8” in Sicilia-Aguilar et al. 2006a) that were not detected at 24 μm (due to our relatively high detection limits at 24 μm). Nevertheless, our recent IRS spectroscopy has confirmed as TO the two TOe8 observed, which together with the facts that no such objects were found in NGC 7160, and that at least one is actively accreting (24-1796), suggested that they are real TO. Summing up the number of “e8” TO, the TO fraction in Tr 37 (including accreting and non-accreting TO) would be closer to $\sim 20\%$ of the total number of disks (or $\sim 10\%$ of the total number of stars), and roughly half (9/20) of the TO are accreting.

Figure 1 does not reveal any strong trend of the accretion rate with the SED slope α . The Spearman rank correlation coefficients (r) and probability of obtaining such r from randomly distributed data (p) for \dot{M} versus α at different wavelengths vary between 0.01 and ± 0.3 (for r) and

0.97-0.02 (for p ; see Table 4). There is a moderate correlation between the slope α in the innermost disk ($3.6\text{-}5.8\mu\text{m}$) and the accretion rates ($r=0.38$, $p=0.02$), which disappears at intermediate wavelengths, and becomes a weak anticorrelation ($r=-0.26$, $p=0.12$) for $\alpha(8.0\text{-}24)$. The $24\mu\text{m}$ photometry was not deep enough to detect photospheres of solar-type stars at these wavelengths, but given the dispersion of the accretion rates for the objects detected and non-detected at $24\mu\text{m}$, we do not believe that the inclusion of objects with undetected $24\mu\text{m}$ fluxes would change the conclusions. This suggests that, in general, objects with more evolved inner disks⁴ tend to have smaller accretion rates. This correlation would be expected if the changes in the dusty disk reflected the evolution of the total surface density, with the dusty and gaseous components evolving “in parallel” (Sicilia-Aguilar et al. 2006b; Fedele et al. 2009). Nevertheless, the fact that most of the Tr 37 disks are substantially evolved and do not have large accretion rates make this trend weak.

Therefore, we find that the objects with the highest accretion rates tend to have the most flared disks, and that there are no TO with $\dot{M} > 10^{-8} M_{\odot} \text{ yr}^{-1}$. Nevertheless, the distribution of accretion rates of TO and CTTS disks are not significantly different (within the limitations of small number statistics; see Section 3.3), and the median accretion rate is the same for accreting TO and normal CTTS disks ($2 \times 10^{-9} M_{\odot} \text{ yr}^{-1}$ and $3 \times 10^{-9} M_{\odot} \text{ yr}^{-1}$, respectively). Most of the CTTS in Tr 37 have relatively low accretion rates (few times $10^{-9} M_{\odot} \text{ yr}^{-1}$), which makes them indistinguishable of the accreting TO in terms of accretion rate. The large number of CTTS with low \dot{M} suggests that, in general, accretion rates as low as $10^{-9}\text{-}10^{-10} M_{\odot} \text{ yr}^{-1}$ do not necessarily cause the opening of an inner hole, as had been suggested by photoevaporation models (Clarke et al. 2001; Ercolano et al. 2009b).

Nevertheless, about half of the TO do not show U band excess nor $H\alpha$ line broadening, which sets upper limits to the accretion of $\leq 10^{-11} M_{\odot} \text{ yr}^{-1}$, despite having similar disk slopes than the accreting TO (see Figure 1) None of the objects with normal near-IR excess lacks evidence of accretion, which reveals an important difference between TO and normal disks, and points out relevant physical differences between accreting and non-accreting TO, as has also been inferred from near-IR spectroscopy (Salyk et al. 2009). Conversely, accretion in objects without any IR excess at *Spitzer*/IRAC wavelengths (and thus, large holes >10 AU) seems rare. We found one object (13-819) with broad $H\alpha$, a measurable accretion rate, and no excess down to $8\mu\text{m}$, although two more objects could represent similar cases (21-895a and 12-1422). Since our MIPS $24 \mu\text{m}$ survey did not detect photospheres of solar-type stars, these objects could still have an excess longwards of $8\mu\text{m}$ and thus a disk with a few-AU hole.

⁴Note that TO and objects with “kink” SEDS have the largest (often positive) $\alpha(8.0\text{-}24)$ slopes in the sample.

3.2. Accretion evolution and the \dot{M} vs. M relation

In the light of the new data for Cep OB2, we examine the time evolution of the accretion rate and the \dot{M} vs M relation. Accretion rates for T Tauri disks are thought to decrease with time in a way that is consistent with the evolution of a viscous disk (Hartmann et al. 1998; Muzerolle et al. 2000; Sicilia-Aguilar et al. 2005b, 2006b). Figure 2 shows the accretion rates of the Cep OB2 objects versus their individual ages, compared to the values measured in other regions: Taurus, ρ Ophiuchus, Chamaeleon I, and TW Hya (Muzerolle et al. 2000), and the Orion L 1630N and L 1641 clouds (Fang et al. 2009), and to the predictions of viscous disk evolutionary models (Hartmann et al. 1998). Although the ages of individual objects are uncertain, given the presence of unresolved binaries and the stellar variability, the global age differences between regions are real. For the G-type stars, the uncertainties in the birthline (Hartmann 2003) result in uncertain ages. Since G-type stars also have more massive disks and higher accretion rates, and our sample contains very few stars earlier than K0 (the median spectral type is K7), we study the time variation of the accretion rate concentrating on objects with spectral types K-M2 only.

The Cep OB2 data in Figure 2 are consistent with the picture of viscous disk evolution, finding a moderate correlation between \dot{M} and age ($r \sim 0.32$, $p = 0.03$). Although the ages of individual objects in Tr 37 are uncertain, the global age spread in Figure 2 is real, as there is a younger (~ 1 Myr) population in Tr 37, associated to the IC 1396A globule, and an age gradient throughout the cluster (Sicilia-Aguilar et al. 2005b). Including the rest of regions above mentioned, the picture of viscous evolution becomes more clear, and the correlation between age and \dot{M} becomes very strong ($r \sim 0.60$, $p < 0.001$). The large range of \dot{M} displayed by objects with a similar age confirms that accretion (and disk) evolution does not happen in the same way in all objects: At any given age, there are many objects that do not have disks and are not accreting. In Tr 37, the number of non-accreting stars is similar to the number of accretors. The initial disk mass and viscosity law affect $\dot{M}(t)$, but viscous evolution alone would not result in so many diskless stars at intermediate ages. Photoevaporation may contribute to remove large amounts of gas and shorten the disk lifetimes (Clarke et al. 2001; Alexander et al. 2006b; Gorti et al. 2009).

Although the accretion data in Cep OB2 and other regions are roughly consistent with viscous evolution (Figure 2), some differences observed provide clues about the different processes that result in disk evolution and dissipation, as well as the typical disk characteristics. The global distribution of accretion rates suggests that the initial disk mass, which controls the initial \dot{M} and thus results in higher or lower accretion rates throughout the time, is higher than the $0.1 M_{\odot}$ assumed by Hartmann et al. (1998)⁵. This disk mass had been calculated from millimeter observations, and we know now that they are probably underestimated by up to an order of magnitude (Andrews & Williams 2007). An initially higher disk mass by a factor of 2-3 would thus be more consistent with the accretion rates we observe in Tr 37 (see Figure 2). The mass would be even higher if we

⁵Note that an initial disk mass $\sim 0.1 M_{\odot}$ results in a disk mass comparable to the minimum mass for the solar nebula, $\sim 0.01 M_{\odot}$ at 1 Myr age.

consider photoevaporation in addition to viscous evolution, since up to 50% of the initial disk mass may be lost via photoevaporation (Gorti et al. 2009). In addition, the typical decay of \dot{M} over time seems slower than previously assumed in the models ($\dot{M} \sim t^{-\eta}$, with $\eta \sim 1.2$ rather than 1.5-2.8 as proposed by Hartmann et al. 1998). This is probably related to the fact that after ~ 4 Myr, only the most massive disks survive, while most of the others have been dissipated by a combination of viscous evolution and photoevaporation (Alexander et al. 2006b; Gorti et al. 2009). The slower decay we observe in our \dot{M} versus age plot also suggests that the long-surviving disks may be biased towards certain radial viscosity laws. In fact, this would be in good agreement with recent observations of Isella et al. (2009) which also revealed a large variety in the viscosity parameter radial exponent for different solar-type objects.

Regarding the relation between the accretion rate and the stellar mass (Figure 3), our results are consistent with a moderate correlation between stellar mass and accretion rate ($r \sim 0.32$, $p = 0.03$) with the slope range observed in Taurus (Calvet et al. 2004), although our sample has systematically lower accretion rates. Our data are also consistent with the $\dot{M} \propto M_*^a$ relation, with $a \sim 2-3$, as has been suggested by Muzerolle et al. (2003), Natta et al. (2004) and, more recently, by Fang et al. (2009), who found a larger index ($a \sim 3$) for the lower-mass stars. Nevertheless, the small mass range spanned by the Cep OB2 objects does not allow us to estimate the value of a , and the fact that U band is less efficient detecting low accretion rates of early K-G stars may also introduce an important bias.

3.3. Accretion in TO: Constraining the origin of the “inner holes”

TO and, in general, evolved disks, are a key factor to understand disk dissipation. Several mechanisms have been invoked to produce a TO disk, but the contribution of each one is not yet understood. The most important ones seem to be photoevaporation (Clarke et al. 2001; Alexander et al. 2006a,b, 2007; Gorti et al. 2009), dust coagulation (Ciesla 2007), and planet formation (Quillen et al. 2004; Edgar et al. 2007). Photoevaporation sets strong constraints to the lifetime and accretion rates of the disk, while strong dust coagulation and planet formation are more flexible. In addition, the inner holes of some TO disks may not be related to pure disk evolution, but to the presence of close-in binaries (Ireland & Kraus 2008). Although TO tend to be rare, summing up to 5-10% of the total number of disks (Hartmann et al. 2005; Fang et al. 2009), some low-mass star forming regions like the Coronet cluster, the MBM12 region, and the η Cha cluster display very high number of TO and evolved disks (Sicilia-Aguilar et al. 2008b; Meeus et al. 2009; Megeath et al. 2005; Sicilia-Aguilar et al. 2009). Although the lack of near-IR excess in very low-mass objects is not a clear sign of a clean inner hole, but may be also reproduced by very flattened/settled disks around low luminosity stars (Ercolano et al. 2009a), the structural differences between these TO and the normal, flared disks are obvious and suggest a strong degree of evolution. In older regions, the number of objects that seem to be “in transition” between Class II and Class III sources, including those with flattened/coagulated/settled inner disks, is higher than expected if

the mechanisms leading to inside-out disk clearing operated in less than a Myr (Currie et al. 2009).

In order to contrast the TO properties at different ages, we examined several well-known regions at different stages of evolution, restricting ourselves to the range of solar-type stars (late G-M2). In Tr 37 the median accretion rate of the CTTS (based on 46 objects) is $\dot{M} = 3 \times 10^{-9} M_{\odot} \text{ yr}^{-1}$, which is not significantly different from the median accretion rate of accreting TO ($\dot{M} = 2 \times 10^{-9} M_{\odot} \text{ yr}^{-1}$, based on 9 objects). In Taurus, the median accretion rates of CTTS (based on 42 objects) and TO (9 objects) differ by one order of magnitude, being $\dot{M} = 3 \times 10^{-8} M_{\odot} \text{ yr}^{-1}$ for CTTS and $\dot{M} = 3 \times 10^{-9} M_{\odot} \text{ yr}^{-1}$ for TO (Najita et al. 2007). In the L 1630N and L 1641 Orion clouds, Fang et al. (2009) gives a similar accretion rate, $\dot{M} = 3 \times 10^{-9} M_{\odot} \text{ yr}^{-1}$, for both CTTS and TO with spectral types G-M6, but if we restrict ourselves to the solar-type range, we find median accretion rates of $\dot{M} = 1 \times 10^{-8} M_{\odot} \text{ yr}^{-1}$ for CTTS and $\dot{M} = 7 \times 10^{-9} M_{\odot} \text{ yr}^{-1}$ for TO (for 88 and 8 stars, respectively). Histograms of the accretion rates of CTTS and TO in the different regions are displayed in Figure 4. Taurus and the Orion clouds have roughly the same ages (1-2 Myr), but the differences between the accretion rate of TO and CTTS in Orion is rather a factor $\lesssim 2$ (thus similar to Tr 37, within small number statistics) than a factor 10. The accretion rates of TO in the work of Najita et al. may be underestimated, since they include upper limits to some TO that are most likely not accreting (like CoKu Tau/4; D’Alessio et al. 2005; Ireland & Kraus 2008), while Fang et al. excludes the non-accreting TO ($\dot{M} < 10^{-11} M_{\odot} \text{ yr}^{-1}$) from the median, as we do here. The way \dot{M} is derived is different in Fang et al. (2009), who estimate the accretion rate from the $H\alpha$ luminosity, compared to Najita et al. (2008), who use accretion rates derived from veiling and U band excess, which are expected to match our work here. Nevertheless, the $H\alpha$ luminosity vs. \dot{M} calibration of Fang et al. (2009) was done using objects whose accretion had been measured from UV veiling and/or U band excess (Gullbring et al. 1998; Dahm 2008; Herczeg & Hillenbrand 2008), so we expect no systematic offsets when comparing the different datasets.

We find differences in the distribution of accretion rates of normal CTTS and TO in the three regions (see Figure 4). The relative numbers of TO that do not show accretion indicators are also different, being higher in Tr 37 than in Orion ($\sim 50\%$ versus $\sim 30\%$; Fang et al. 2009). In Tr 37, the fact that we find normal CTTS with low \dot{M} and TO with similar accretion rates suggests that the difference in near-IR excess for these two types of sources is related only to the dust content (grain growth/dust settling), without significant differences in the gaseous disk component. In addition, the difference in the accretion rates of TO in regions with different ages is not as striking as the evolution seen for CTTS (see Figures 2 and 4). This could be understood if the mechanisms producing the holes of TO require a special range of accretion rates to be effective, or if the changes produced in the disk structure of TO constrain the allowed range of \dot{M} .

The order of magnitude difference between the accretion rates of CTTS and TO (for similar disk masses) observed by Najita et al. in Taurus is consistent with the opening of holes by Jovian planet formation. The predictions for the changes in the accretion rate with the presence of a planet suggest that the accretion through the gap is about 10% of the accretion through the outer disk (Lubow & D’Angelo 2006). Viscous evolution would proceed relatively undisturbed after the

formation of a planet (Mordasini & Klahr, private communication), and thus the accretion rates of TO would be expected to evolve with time as the accretion for normal CTTS disks does. Therefore, the lack of differences and \dot{M} evolution seen in Tr 37 suggests that most of the accreting TO in this region are not related to giant planet formation. Planet synthesis models (Mordasini et al. 2009) predict that planet formation in disks with typical masses would peak at an age ~ 4 Myr, so we may expect a large number of planet-related holes at the age of Tr 37. Nevertheless, the mass distribution of observed planets (Bouchy et al. 2009) indicates that most of these objects would have masses insufficient to open a clean hole, or too large to allow accretion to continue. Therefore, we may expect that most of the disks harboring planets in Tr 37 would show either normal IR excess, or be otherwise non-accreting TO.

The timescales for the onset of the different disk-clearing mechanisms (close-in binaries, photoevaporation, strong grain coagulation/settling, and/or planetesimal/planet formation) are not the same, and the lifetimes of the resulting objects are also different. Therefore, it is not evident that the bulk of TO in regions with different ages ought to contain physically similar objects. Rapid formation of a giant planet in a gravitationally unstable inner disk is nearly instantaneous (Boss 1997), although only a minority of disks may be massive enough to suffer gravitational instability (Andrews & Williams 2007). A hole due to the presence of a binary companion would appear also immediately, but the resulting circumbinary disk is expected to survive less than a disk around a single star, with a lifetime ~ 5 Myr (Bouwman et al. 2006). Photoevaporation (Clarke et al. 2001) is efficient only in combination with viscous evolution (Gorti et al. 2009), but it produces an inner hole only if the accretion rate falls below a certain limit and the disk mass is low enough⁶. The lifetimes of the resulting TO are expected to be of the order of few hundred thousand years (Alexander et al. 2006a,b; Gorti & Hollenbach 2009). Other studies involving time-dependent disk evolution and X-ray/FUV/EUV photoevaporation predict inner hole opening starting at ~ 4 Myr, and TO lifetimes that can exceed 1 Myr (Gorti et al. 2009), although accretion would drop to undetectable levels shortly after the opening of the hole. Photoevaporation also depends strongly on the structure of the disk and the dust (Gorti & Hollenbach 2009, Gorti et al. 2009; Ercolano et al. 2009b). The lower irradiation in flattened (geometrically thin) disks decreases the efficiency of photoevaporation, while grain growth decreases the opacity of the disk and thus favors photoevaporation. The combined result of these two opposite effects is unclear, and probably depends on the individual disk parameters (U. Gorti, private communication). Some observational studies have suggested that strong mass removal by photoevaporation may only be efficient at a late stage in the disk evolution (Pascucci & Sterzik 2009), as has been also proposed theoretically (Alexander & Armitage 2009). The theoretical timescales for dust coagulation are uncertain (Dullemond & Dominik 2005; Brauer et al. 2008; Birnstiel et al. 2009), but observations suggest an important degree of dust evolution in the disks of solar-type stars by the age of ~ 4 -5 Myr (Sicilia-Aguilar et al. 2006a; Rodmann et al. 2006; Currie et al. 2009).

⁶Note that X-ray+FUV photoevaporation, combined with viscous disk evolution, is efficient removing a large fraction of the disk mass in a few Myr even if no hole is created.

The systematically flatter disks in Tr 37 (compared to Taurus) and the similar accretion rates of accreting TO and normal CTTS are consistent with most TO in Tr 37 resulting from strong grain coagulation that leaves the gas content (and accretion) relatively unchanged. The implications of the lack of statistical differences in the accretion rates of accreting TO and normal disks in Tr 37 are multiple. On one hand, significant amounts of matter must be crossing the depleted inner disks of accreting TO, which favors the scenario where the near-IR hole has been created by planetesimal formation/strong grain coagulation, rather than being due to gas removal by photoevaporation. A picture where the small dust has been strongly or even totally removed, but the gas flow continues more or less undisturbed, seems more complicated to achieve than a situation where the whole inner disk has been cleared from dust and gas. Several mechanisms, like dust filtration at the edges of a gap created by a planet (Rice et al. 2006) and the differences in turbulence/coagulation between active and dead zones in layered disks (Ciesla 2007) have been proposed to produce radially-dependent dust distributions and optically thin inner disks. Radially dependent grain coagulation and settling are also consistent with the typical SEDs seen in the CTTS members of Tr 37, many of which show a change of slope or “kink” around $6\text{-}8\mu\text{m}$ (Sicilia-Aguilar et al. 2006a). Non-accreting TO in Tr 37 cannot be explained by grain coagulation alone, but require a mechanism to remove the gas or at least, not to allow the gas transport into the inner disk. Binary companions could be a good candidate, although we would expect few surviving circumbinary disks at 4 Myr age (Bouwman et al. 2006), and recent surveys of TO suggest that binaries as the cause of TO are the exception and not the rule (Pott et al. 2009). Photoevaporation may only be efficient for the most flared objects, but strong grain coagulation may help to photoevaporate the gas in the innermost regions once the dust opacity decreases sufficiently. Finally, the formation of one or more giant planets may reduce the typically low accretion rates of CTTS in Tr 37 below our detection limits, which could explain at least part of our non-accreting TO.

In addition, initial conditions, that have been invoked to explain the spread in the \dot{M} vs. M_* relation (Dullemond et al. 2006), could also determine the types of disks and TO that dominate in a given cluster. The quiescent, undisturbed environment in Taurus may affect both the evolution of the disks, compared to OB associations like Orion L 1630N and L 1641 clouds or Tr 37, as well as the initial conditions at the time of formation (and thus, initial disk masses and sizes).

3.4. Accretion variability: How common are EX-or objects?

Young pre-main sequence stars are known to be variable, with most variations due to the combination of rotation and cool spots (type I variability), hot spots and changes in the accretion rate (type II variability), and obscuration by circumstellar dust (type III variability; Herbst et al. 1994; Hillenbrand et al. 1998). In the case of accreting stars, variations up to 0.5 magnitudes at optical wavelengths in timescales of a few days are common, suggesting that the accretion flow is variable (Bertout 1989; Briceño et al. 2001; Eiroa et al. 2002). Variable accretion has been also suggested by the changes in the accretion-related emission lines (both in line profile and

in EW; Alencar et al. 2001; Alencar & Batalha 2002; Sicilia-Aguilar et al. 2005a). Accretion variability is more dramatic in the case of EX-or objects, which experience repeated outbursts of different magnitude in timescales of months to decades (Hartmann & Kenyon 1996; Herbig et al. 2001; Herbig 2007, 2008). Some particularly bright outbursts may be strong enough to trigger the formation of crystalline dust throughout the disk (Ábrahám et al. 2009), which could explain the abundance of crystals in the comets in our own Solar System. It has been suggested that the EX-or phase should be common for young stars (Hartmann & Kenyon 1996; Hartmann 1998), but the actual fraction of objects suffering accretion variability is uncertain, especially because the typical variations may be too small (<2 mag) to be noticed in more distant clusters and associations.

We have discussed in detail the variability of the Tr 37 member GM Cep (also known as 13-277 in our member list; Sicilia-Aguilar et al. 2008a). Taking just into account our previous optical data (Sicilia-Aguilar et al. 2004, 2005b) and our new photometry, we find that more than 10% of the stars display variations in V of at least 0.5 magnitudes (see Table 2). Given that we compare here only two epochs, we expect that many more of the cluster members regularly display variability with $\Delta V \geq 0.5$ mag. A lower degree of variability, $\Delta V \geq 0.1$ mag is even more common, with 2/3 (65%) of the objects showing such changes. Among the 8 objects with double measurements in our LAICA survey, we do not observe significant variations between the \dot{M} measured on consecutive days. Despite the limitations of our FLWO observations, we have compared our previous accretion rates with the new values, in order to look for accretion variability and optical variability in general. Several objects display significant variations in their accretion rates, which can be confirmed in two cases by optical spectroscopy:

The CTTS 11-2146 shows now an accretion rate $\dot{M} \sim 10^{-8} M_{\odot} \text{ yr}^{-1}$, more than one order of magnitude below the one measured previously ($\dot{M} \sim 1.7 \times 10^{-7} M_{\odot} \text{ yr}^{-1}$). The variability of the object, and maybe the presence of a nearby ($2''$) accreting star, could have affected our less sensitive U band measurements at the FLWO, but available high-resolution spectra taken with HIRES in 2001 (for details about the HIRES data, see Sicilia-Aguilar et al. 2008a) and Hectochelle in 2004 (Sicilia-Aguilar et al. 2006b) are in agreement with \dot{M} variations (Figure 5). The spectroscopic data reveals changes in the emission line profile as well as in the blueshifted absorption, associated to variable accretion plus wind.

The star 14-141 appears to have suffered an increase in its accretion rate, compared to our previous observations, where it was not detected. The comparison of HIRES 2001 data with Hectochelle spectra taken in 2004 confirms a very strong $H\alpha$ variability, with remarkable changes in the line profile (Figure 5). The $H\alpha$ profile in 2001 was dominated by a shock, being that of a Herbig Haro object (also confirmed by the presence of forbidden [N II] and [S II] emission; Hartigan et al. 1987). By 2004, the signs of shock are much weaker, and the profile appears to be typical for an accreting CTTS, with a blueshifted absorption indicative of a wind/outflow.

Although we do not have multiepoch high-resolution spectroscopy for the rest of the objects, several other stars are candidates for strong optical variability maybe related to accretion vari-

ations: 13-1238, 13-236, 13-1250, 53-1762, 21-1762, 11-2031, and 82-272 (see Table 5). These objects are good candidates to look for EX-ors and explore the typical variability in accreting solar-type stars. In addition, we find a TO with narrow H α in 2004, and evidence of accretion ($0.11^{+0.23}_{-0.06} \times 10^{-8} M_{\odot} \text{ yr}^{-1}$) in 2007, 72-875. The star is probably a single-lined spectroscopic binary, so episodic accretion may be a possibility. Although a few TO display accretion-related variability (13-1250, 21-1762, 72-875), we must stress that the most remarkable cases of \dot{M} variability correspond to stars with the most flared and most massive disks (13-277) and objects associated to the younger (~ 1 Myr) part of the cluster (11-2146, 14-141).

Finally, we must mention that several objects are consistent with type III variability, displaying changes in the extinction larger than expected from the typical errors. While U and VRI were not simultaneous in our FLWO survey, the three bands VRI were taken within 30 min to 1 hour difference, so the A_V estimates are as robust as the A_V derived from LAICA observations. Comparing the A_V values in Sicilia-Aguilar et al. (2004, 2005b) with the LAICA ones, we find several type III variability candidates: 14-287, 11-581, 13-1048, 11-1067, 82-272, 12-1955, 12-595, 21-840, 21-230, 21-1692, 21-763, 21-1762, and 11-2146 (see Table 6). Among these, 14-287, 13-1048, 82-272, 12-595, 21-840, and 11-2146 have circumstellar disks that could be responsible for the extinction variations. Therefore, the variability of 11-2146 could be a combination of type II and type III variability. The stars 13-1048 (M0), 82-272 (G9, SB2 with two similar-mass accreting components), and 12-595 (K7) have such dramatic A_V changes that might be considered as good candidates for UX-or variables. In the case of 12-595, the anomalous optical colors (with a too blue V-I color for a K7 star, responsible for the anomalous age derived from the isochrones) are consistent with a nearly edge-on disk where scattering is an important contributor to the measured luminosity.

4. Summary and conclusions

We present new optical (UVRI) photometry for the Tr 37 and NGC 7160 clusters in the Cep OB2 region. The data allow us to constrain the presence of accretion and accretion rates in more than 60 T Tauri stars with evolved disks, including 20 TO with zero or very small near-IR excess and presumably, inner holes and/or coagulated/settled inner disks. We study the dependence of the accretion rate on the disk structure (using the SED slope, α , as an indicator of the structure of the disk) finding no strong correlation between α at different wavelengths and the accretion rate. In fact, although we do not find any TO with a large ($>10^{-8} M_{\odot} \text{ yr}^{-1}$) accretion rate and the most flared disks have typically the largest accretion rates, strong accretors are rare in regions as old as Tr 37, and we do not see any statistically significant difference between the accretion rates of TO and normal CTTS disks. This result is in contrast with the observations of Taurus (Najita et al. 2007), which reported that accretion rates for TO are systematically biased towards lower values of \dot{M} , with accretion rates about one order of magnitude lower than the typical CTTS accretion rates for a similar disk mass. We must stress that the accretion rates of TO in Taurus are similar to those of TO in Cep OB2, with the difference being that CTTS in Tr 37 have typical accretion

rates about one order of magnitude lower than Taurus CTTS. Nevertheless, about half of the TO do not show any evidence of accretion, which suggests that the TO class includes several different types of objects and physical processes.

The formation of Jovian planets is expected to cause inner holes and reduce the accretion rate onto the star compared to normal CTTS disks (Lubow & D’Angelo 2006; Najita et al. 2007). On the other hand, photoevaporation by X-ray, EUV, and FUV photons predicts in general a smaller fraction of TO (especially, a much lower fraction of accreting TO) and the opening of a hole would happen only when the accretion rate drops below a certain limit (10^{-9} - 10^{-10} M_{\odot} yr^{-1} ; Alexander et al. 2006b), which also differs from our observations. Nevertheless, the efficiency of photoevaporation may be reduced if the disk flaring is low, as is the general case in Cep OB2. New models suggest larger lifetimes for photoevaporated TO ($\gtrsim 1$ Myr; Gorti et al. 2009), but predict a short lifetime of accretion once the hole has been opened. Other physical processes, like strong coagulation of the dust, may also result in optically thin inner disks with relatively normal accretion rates.

Given the different timescales for the onset of the various disk clearing mechanisms and the expected lifetimes of each type of TO, it is not evident that the TO in all regions are physically the same type of objects. The fact that physically different types of TO may dominate at different ages has been recently suggested from a theoretical point of view (Alexander & Armitage 2009). Their models suggest that accreting TO are expected to contain planets, while most non-accreting TO should have been produced by photoevaporation. They also claim that at young ages (< 2 Myr, similar to Taurus), TO will be dominated by planet formation, while at older stages (> 6 Myr), photoevaporation should be the main responsible for TO. Here we find that in an intermediate-aged cluster like Tr 37, the similarity of the accretion rates of CTTS and TO are consistent with most of the accreting TO being related to strong grain coagulation and settling. In the case of the TO that do not show any evidence of accretion, other mechanisms, like the presence of companions (stellar/substellar), giant planet formation, and/or photoevaporation, may be responsible for their inner holes. The fact that the fraction of non-accreting TO in Tr 37 is higher ($\sim 50\%$) than in younger regions like Orion ($\sim 30\%$; Fang et al. 2009) would also be in agreement with photoevaporation becoming more efficient at older ages (Alexander & Armitage 2009).

Finally, we explore stellar variability with our very limited two-epoch UVRI observations, finding that $\sim 10\%$ of the stars show magnitude variations with $\Delta V \geq 0.5$ mag, and $\sim 65\%$ have $\Delta V \geq 0.1$ mag. Several cases are compatible with type II variability (or increased accretion episodes, as in EX-or objects), and many others show important variations in their extinction, suggesting type III or UX-or-like variations, sometimes added to a variable accretion. The relatively large number of type II variables found with data from only two epochs suggests that accretion variations are very common among young stars. Although the most remarkable accretion variations occur in the younger stars with more massive disks, we also observe accretion variability in some TO. Large variations in the accretion rate could be an important mechanism to produce crystalline silicates as those found in the Solar System (Ábrahám et al. 2009).

Acknowledgments: We want to thank U. Gorti for the insight and discussion about photoevaporation, especially for the cases of evolved disks, and M. Fang for providing the accretion data in the Orion suburbs. We are also indebted to C. Mordasini and H. Klahr for the discussion about the evolution of disks after planet formation, and the anonymous referee for a detailed review of our paper that helped clarifying this work. We are also grateful to B. Braunecker and F. Hormuth for their help at the 70 cm Königstuhl telescope, as well as the service mode observers in Calar Alto, S. Pedraz and J. Aceituno. We finally thank L. Hillenbrand for providing the HIRES spectra of the objects 11-2146 and 14-141. A.S-A. acknowledges support from the Deutsche Forschungsgemeinschaft, DFG, grant number SI 1486/1-1. Based on observations collected at the Centro Astronómico Hispano Alemán (CAHA) at Calar Alto, operated jointly by the Max-Planck Institut für Astronomie and the Instituto de Astrofísica de Andalucía (CSIC). This work makes use of data products from the Two Micron All Sky Survey, which is a joint project of the University of Massachusetts and the Infrared Processing and Analysis Center/California Institute of Technology, funded by the National Aeronautics and Space Administration and the National Science Foundation.

REFERENCES

- Ábrahám, P., Juhász, A., Dullemond, C.P., Kóspal, A., van Boekel, R., Henning, Th., Moór, A., Mosoni, L., Sicilia-Aguilar, A., Sipos, N., 2009, *Nature* 459, 224
- Adams, F., Lada, C., Shu, F., 1987, *ApJ*, 312, 788
- Alencar, S., Johns-Krull, C., Basri, G., 2001, *AJ* 122, 3335
- Alencar, S., Batalha, C., 2002, *ApJ* 571, 378
- Alexander, R., Clarke, C., Pringle, J, 2006a *MNRAS*, 369, 216
- Alexander, R., Clarke, C., Pringle, J, 2006b *MNRAS*, 369, 229
- Alexander, R., & Armitage, P., *ApJ* in press
- Andrews, S., & Williams, J., 2007, *ApJ*, 671, 1800
- Apai, D.; Pascucci, I.; Bouwman, J.; Natta, A.; Henning, Th.; Dullemond, C. P., 2005, *Sci*, 310, 834
- Bertout, C., 1989, *ARAA*, 27, 351
- Birnstiel, T., Dullemond, C., Brauer, F., 2009, *A&A* in press
- Bouchy, F., Mayor, M., et al., 2009 *A&A* 496, 527

- Bouwman, J.; Lawson, W. A.; Dominik, C.; Feigelson, E. D.; Henning, Th.; Tielens, A. G. G. M.; Waters, L. B. F. M., 2006, *ApJ*, 653, 57
- Boss, A. P. 1997, *Science*, 276, 1836
- Brauer, F., Dullemond, C. P., & Henning, T. 2008, *A&A*, 480, 859
- Briceño, C., et al. 2001, *Science*, 291, 93
- Calvet, N., Muzerolle, J., Briceño, C., Hernández, J., Hartmann, L., Saucedo, J. L., & Gordon, K. D. 2004, *AJ*, 128, 1294
- Cardelli, J., Clayton, G., Mathis, J., 1989, *ApJ*, 345, 245
- Carmona, A., van den Ancker, M., Henning, Th., Goto, M., Fedele, D., Stecklum, B., 2007, *A&A* 476, 853
- Carmona, A., van den Ancker, M., Henning, Th., Pavlyuchenkov, Y., Dullemond, C.,
- Carr, J., Mathieu, R., Najita, J., 2001, *ApJ*, 551, 454
- Ciesla, F., 2007, *ApJL* 654, 159
- Clarke, C., Gendrin, A., & Sotomayor, M., 2001, *MNRAS* 328, 485
- Clarke, C., & Pringle, J., 2006, *MNRAS*, 370, L10
- Contreras, M.E., Sicilia-Aguilar, A., Muzerolle, J., Calvet, N., Berlind, P., Hartmann, L. 2002, *AJ*, 124, 1585
- Currie, T., Lada, C., Plavchan, P., Robitaille, Th., Irwin, J., Kenyon, S., 2009, *ApJ* 698, 1
- Dahm, S. E. 2008, *AJ*, 136, 521
- D'Alessio, P., Hartmann, L., Calvet, N., Franco-Hernández, R., and 10 more coauthors, 2005, *ApJ*, 621, 461
- De Graeve, E., 1983, *Vatican Obs. Publ.*, 2, 31
- Dullemond, C., & Dominik, C., 2005, *AA*, 434, 975
- Dullemond, C., Natta, A., Testi, L., 2006, *ApJL* 645, L69
- Edgar, R., Quillen, A., Park, J., 2007, *MNRAS*, 381, 1280
- Eiroa, C., Oudmaijer, R., et al., 2002, *A&A* 384, 1038
- Ercolano, B., Clarke, C., Robitaille, T., 2009a, *MNRAS* 394, L141
- Ercolano, B., Clarke, C., Drake, J., 2009b, *ApJ* 669, 1639

- Fang, M.; van Boekel, R.; Wang, W.; Carmona, A.; Sicilia-Aguilar, A.; Henning, Th., 2009, A&A in press
- Fernie, J., 1983, PASP, 95, 782
- Forrest, W.J., Sargent, B., Furlan, E., & 18 more coauthors, 2004, ApJS, 154, 443
- Gorti, U., & Hollenbach, D., 2009, ApJ690, 1539
- Gorti, U., Dullemond, C., & Hollenbach, D., 2009, ApJin press
- Goto, M., Usuda, T., Dullemond, C., Henning, T., Linz, H., Stecklum, B., Suto, H., 2006, ApJ 652, 758
- Goto, M., Thi, W.F., Bouwman, J., Waters, L.B.F.M., 2008, A&A 477, 839
- Gullbring, E., Hartmann, L., Briceño, C., Calvet, N., 1998, ApJ 492, 323
- Haisch, K., Lada, E., & Lada, C., 2001, ApJ, 553, 153
- Hartigan, P., Raymond, J., Hartmann, L., 1987, ApJ 316, 323
- Hartmann, L.: Accretion Processes in Star Formation, Cambridge University Press, 1998.
- Hartmann, L., & Kenyon, S., 1987, ApJ 322, 393
- Hartmann, L., & Kenyon, S., 1996, ARA&A, 34, 207
- Hartmann, L., Calvet, N., Gullbring, E. & D'Alessio, P, 1998, ApJ, 495, 385
- Hayashi, C., Nakazawa, K., & Nakagawa, Y. 1985, in Protostars and Planets II, eds. D. Black & M. Matthews(Tucson: University of Arizona Press), 1100
- Herczeg, G. J., & Hillenbrand, L. A. 2008, ApJ, 681, 594
- Hernández, J., Hartmann, L., Megeath, S.T., et al., 2007, ApJ, 662, 1067
- Hollenbach, D., Yorke, H., Johnstone, D., 2000, Protostars and Planets IV, Univ. Arizona Press, p. 401
- Ireland, M., & Kraus, A., 2008, ApJ, 678, 59
- Isella, A., Carpenter, J., & Sargent, A., 2009, ApJ 701, 260
- Johansen, A., & Klahr, H., 2005, ApJ, 634, 1353
- Johansen, A., Oishi, J., Mac Low, M.M., Klahr, H., Henning, Th., Youdin, A., 2007, Nature 448, 1022
- Kenyon, S.J. & Hartmann, L., 1987, ApJ, 323, 714

- Kenyon, S.J. & Hartmann, L., 1995, *ApJS* , 101, 117
- Königl, A., *ApJ*, 370, L39
- Lada, C., Muench, A., et al., 2006, *AJ*, 131, 1547
- Lawson, W., Lyo, A., Muzerolle, J., 2004, *MNRAS*, 329, 29
- Lubow, S.H., & D’Angelo, G., 2006, *ApJ*, 641, 526
- Mathieu, R., Adams, F., Latham, D., 1991, *AJ*, 101, 2184;
- McCabe, C., Ghez, A., Prato, L, Duchene, G., Fisher, R., Telesco, C., 2006, *ApJ* 636, 932
- Megeath, S. T.; Hartmann, L.; Luhman, K. L.; Fazio, G. G., 2005, *ApJ*, 634, 113
- Mordasini, C., Alibert, Y., Benz, W., Naef, D., *A&A* 501, 1161
- Muzerolle, J., Calvet, N., Briceño, C., Hartmann, L. & Hillenbrand, L., 2000, *ApJ*, 535, L47
- Muzerolle, J., Hillenbrand, L., Calvet, N., Briceño, C.; Hartmann, L., 2003, *ApJ*, 592, 266
- Muzerolle, J., Allen, L., Megeath, S.T., Hernández, J., Gutermuth, R., 2009, *ApJ* in press, ArXive 0911.2704
- Najita, J., Carr, J., Glassgold, A., Shu, F., Tokunaga, A., 1996, *ApJ*, 462, 919
- Najita, J., Carr, J., Mathieu, R., 2003, *ApJ*, 589, 931
- Najita, J., Strom, S., Muzerolle, J., 2007, *MNRAS* 368, 379
- Natta, A., Testi, L., Neri, R., Shepherd, D., Wilner, D., 2004, *A&A*, 416, 179
- Pascucci, I., Apai, D., Henning, T., Sterzik, M., Dullemond, C., Bouwman, C., 2005, *Mem.S.A.It.*, 76, 315
- Pascucci, I. et al. 2006, *ApJ*, 651, 1177
- Pascucci, I., Apai, D., Luhman, K., Henning, Th., Bouwman, J., Lahuis, F., Natta, A., 2009, *ApJ*, 696, 143
- Pascucci, I., Sterzik, M., 2009, *ApJ*, 702, 724
- Patel, N.A., Goldsmith, P.F., Heyer, M.H. & Snell, R.L., 1998, *ApJ* , 507, 241
- Pott, J.U., Perrin, M., Furlan, E., Ghez, A., Herbst, T., Metchev, S., 2009, *ApJ* in press, arXive 0912.0846
- Quanz, S., Henning, Th., Bouwman, J., Van Boekel, R., Juhasz, A., Linz, H., Pontoppidan, K., Lahuis, F., 2007, *ApJ*, 668, 359

- Quillen, A., Blackman, E., Frank, A., Varniere, P., 2004, ApJ, 612, L137
- Rettig, T., Brittain, S., Gibb, E., Simon, T., Kulesa, C., 2005, ApJ, 626, 245
- Rice, W., Armitage, P., Wood, K., Lodato, G., 2006, MNRAS 373, 1619
- Rodmann, J.; Henning, Th.; Chandler, C. J.; Mundy, L. G.; Wilner, D. J., 2006, A&A, 446, 211
- Salyk, C., Blake, G., Boogert, A., Brown, J., 2009, ApJ, 669, 330
- Schräpler, R. & Henning, Th., 2004, ApJ, 614, 960
- Setiawan, J.; Henning, Th.; Launhardt, R.; Müller, A.; Weise, P.; Kürster, M., 2008, Nature, 451, 38
- Sicilia-Aguilar, A., Hartmann, L., Szentgyorgyi, A., Roll, J., Conroy, M., Calvet, N., Fabricant, D., & Hernández, J., 2005a, AJ, 129, 363
- Sicilia-Aguilar, A., Hartmann, L., Hernández, J., Briceño, C., Calvet, N., 2005b, AJ, 130, 188
- Sicilia-Aguilar, A., Hartmann, L., Calvet, N., Megeath, S.T., Muzerolle, J., Allen, L., D’Alessio, P., Merín, B., Stauffer, J., Young, E., Lada, C., 2006a, ApJ 638, 897
- Sicilia-Aguilar, A., Hartmann, L., Fűrész, G., Henning, Th., Dullemond, C., Brandner, W., 2006b, AJ 132, 2135
- Sicilia-Aguilar, A., et al., 2008a, ApJ 673, 382
- Sicilia-Aguilar, A.; Henning, Th.; Juhász, A.; Bouwman, J.; Garmire, G.; Garmire, A., 2008b, ApJ, 687, 1145
- Sicilia-Aguilar, A., Bouwman, J., Juhász, A., et al., 2009, ApJ, 701, 1188
- Siess, L., Dufour, E. & Forestini, M. 2000 A&A , 358, 593
- Strom, K., Wilkin, F., Strom, S., & Seaman, R., 1989, AJ, 98, 1444
- Van Boekel, R., Waters, L., Dominik, C., Bouwman, J., de Koter, A., Dullemond, C., Paresce, F., 2003, AA, 400, L21
- White, R., & Basri, G., 2003, ApJ, 582, 1109

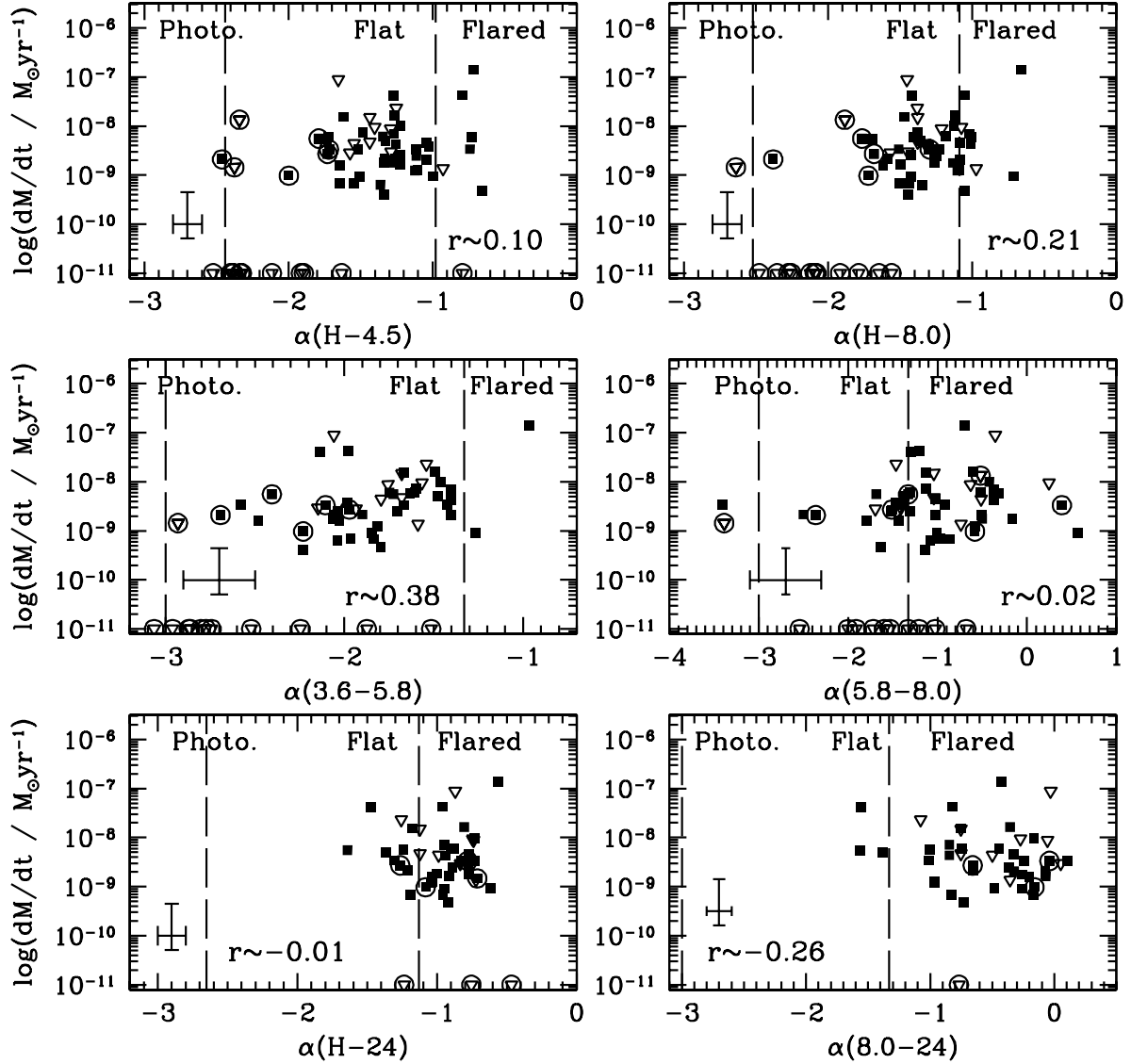


Fig. 1.— Accretion rate versus the disk slope ($\alpha = d \log(\lambda F_{\lambda})/d \log(\lambda)$) at different wavelengths. The slopes of a stellar photosphere (for a K7 star) and an optically thick, geometrically thin disk (Kenyon & Hartmann 1987) are displayed for comparison. Upper limits are shown as inverted open triangles. TO are marked with large circles. The typical error bars, considering a 10% uncertainty in the IRAC photometry, are also displayed. To demonstrate the similarity of slopes between accreting and non-accreting TO, we also display the α values of non-accreting TO, with upper limits to accretion $10^{-11} M_{\odot} \text{yr}^{-1}$ derived from H α spectroscopy. The generalized “inside-out” evolution in Tr 37 (with nearly all objects showing stronger excess at longer wavelengths; Sicilia-Aguilar et al. 2006a) is responsible for the changing α values at different wavelengths for each disk.

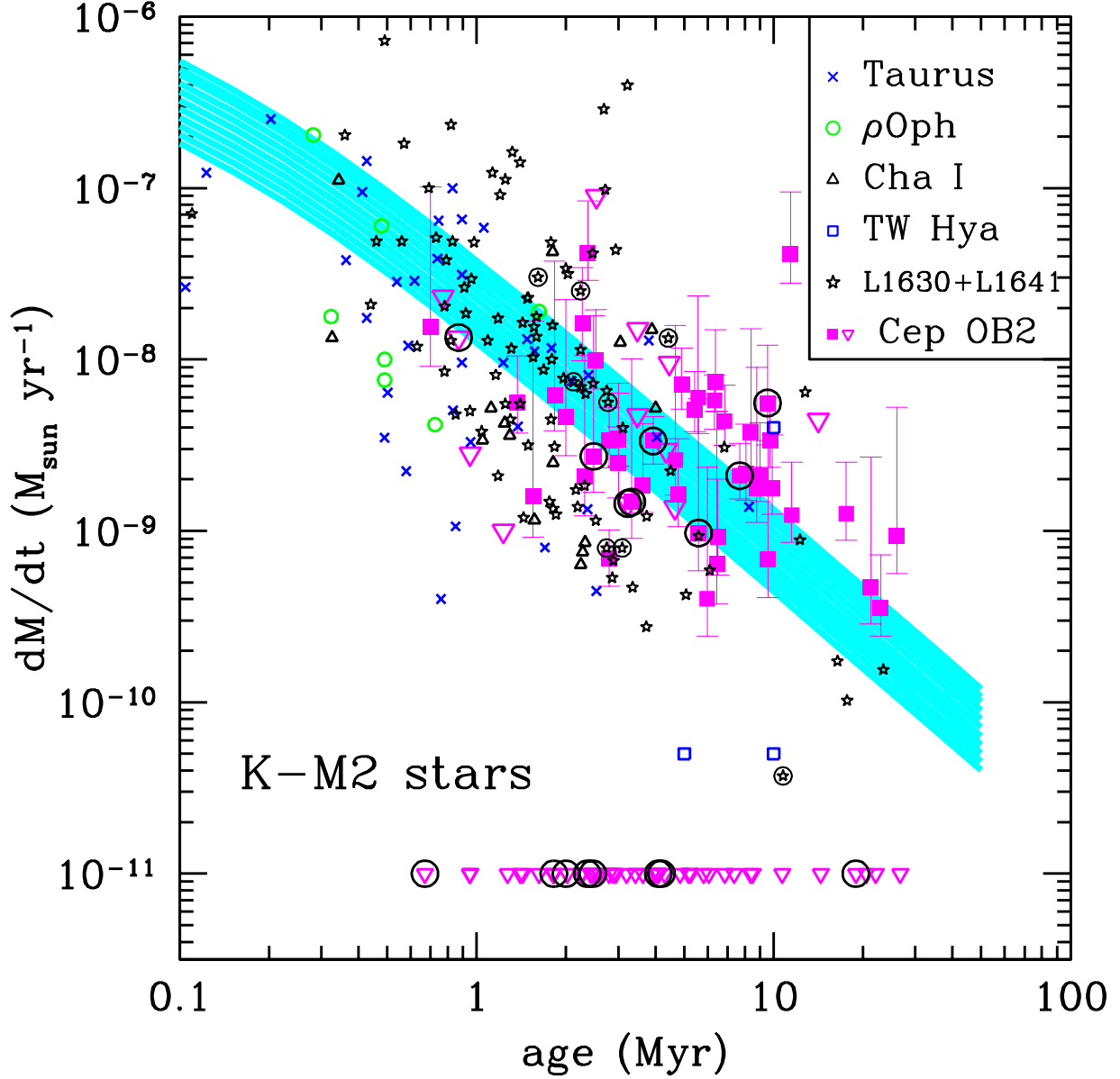


Fig. 2.— Accretion versus stellar age. Detected accretion rates are represented by filled squares. Upper limits are shown as inverted open triangles. The upper limits based on $H\alpha$ spectroscopy ($\dot{M} < 10^{-11} M_{\odot} \text{ yr}^{-1}$ for narrow lines) are also displayed. The plot includes data from other regions (Muzerolle et al. 2000; Fang et al. 2009). We also display a collection of viscous disk evolutionary models (Hartmann et al. 1998) for solar-type stars with initial disk masses $\sim 0.1\text{-}0.2 M_{\odot}$, constant viscosity $\alpha = 10^{-2}$, and viscosity exponent $\gamma = 1$. Note that individual ages have large errors (not shown), mostly due to the presence of unresolved binaries and variability. TO in Cep OB2 and in the Orion L 1630N and L 1641 clouds are marked with a large circle around the corresponding symbol. The Spearman rank correlation coefficient and probability of random distribution for the $\log(\dot{M})$ vs. $\log(\text{age})$ relation are $r \sim 0.60$, $p < 0.001$ (including the stars in all the regions, but excluding the non-accreting objects).

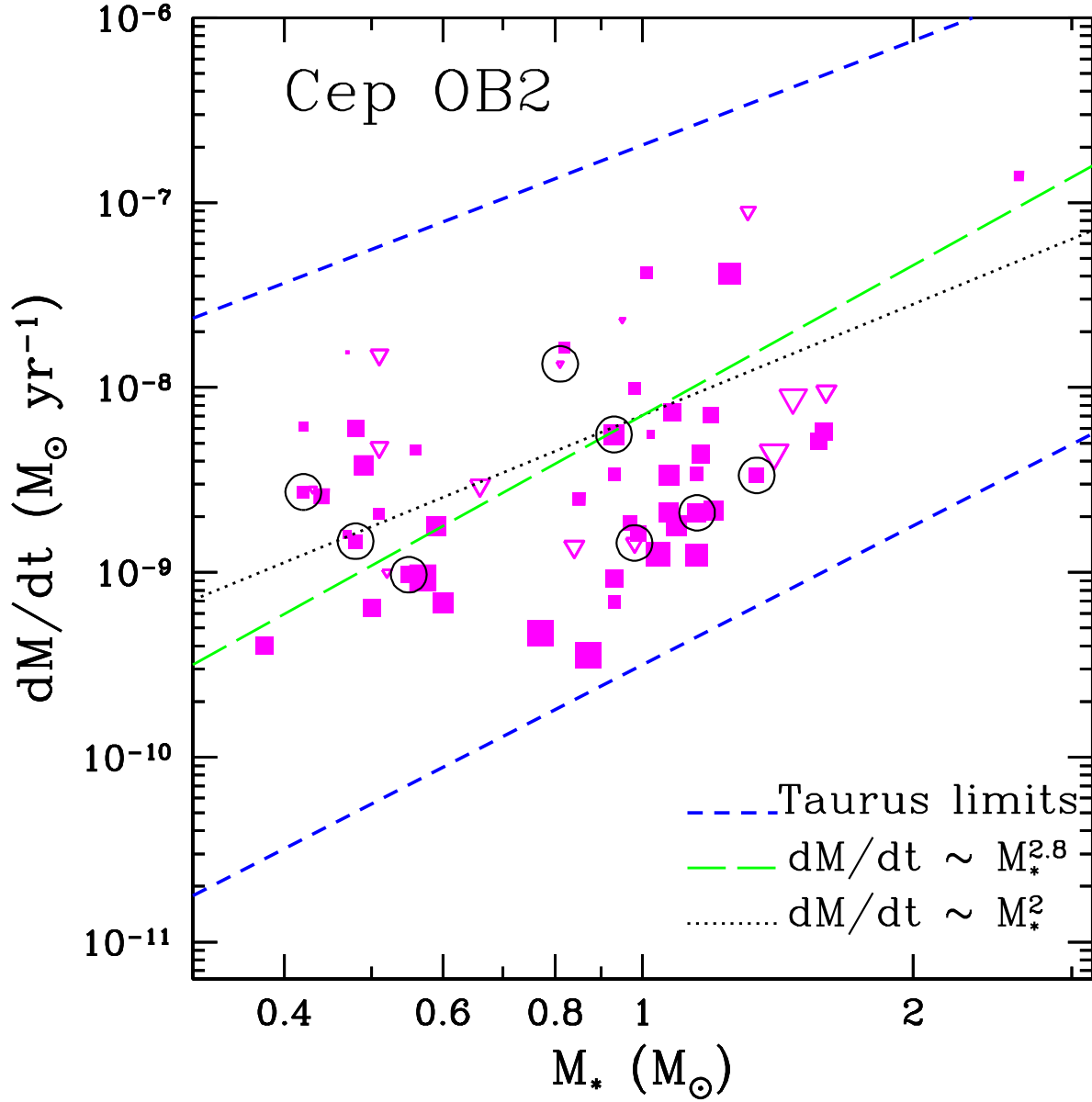


Fig. 3.— Accretion versus stellar mass. Upper limits are shown as inverted open triangles. The size of the symbols is proportional to the individual age (from ~ 1 to ~ 15 Myr). We show the limits of accretion and stellar mass for Taurus stars (short-dashed blue lines; Calvet et al. 2004), the slope for the $\dot{M} \sim M_{*}^2$ relation (dotted black line; Natta et al. 2004), and the slope for $\dot{M} \sim M_{*}^{2.8}$ (long-dashed green line; Fang et al. 2009). Note that these lines are merely indicative and not fits to the data. The Spearman rank correlation coefficient and probability of random distribution for the $\log(\dot{M})$ vs. $\log(M_{*})$ are $r \sim 0.32$, $p = 0.03$.

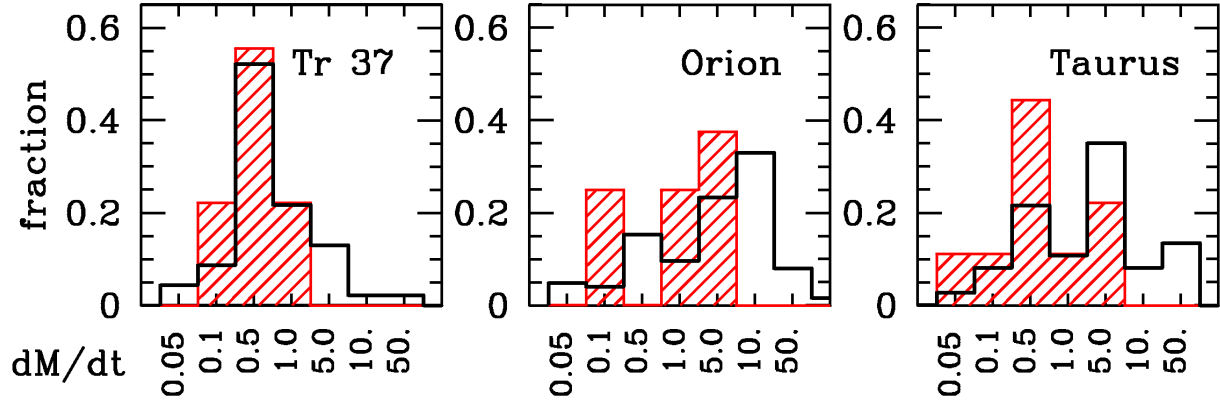


Fig. 4.— Fraction of objects with accretion rates in a given range in Tr 37, the Orion L 1630N and L 1641 clouds, and Taurus. Normal CTTS are displayed in black, the dashed red histogram corresponds to the TO in each region. The mass accretion rate is given in units of $10^{-8} M_{\odot} \text{yr}^{-1}$. The fraction of objects with a given \dot{M} range is normalized to the total number of objects in each class for each region (CTTS and TO, respectively).

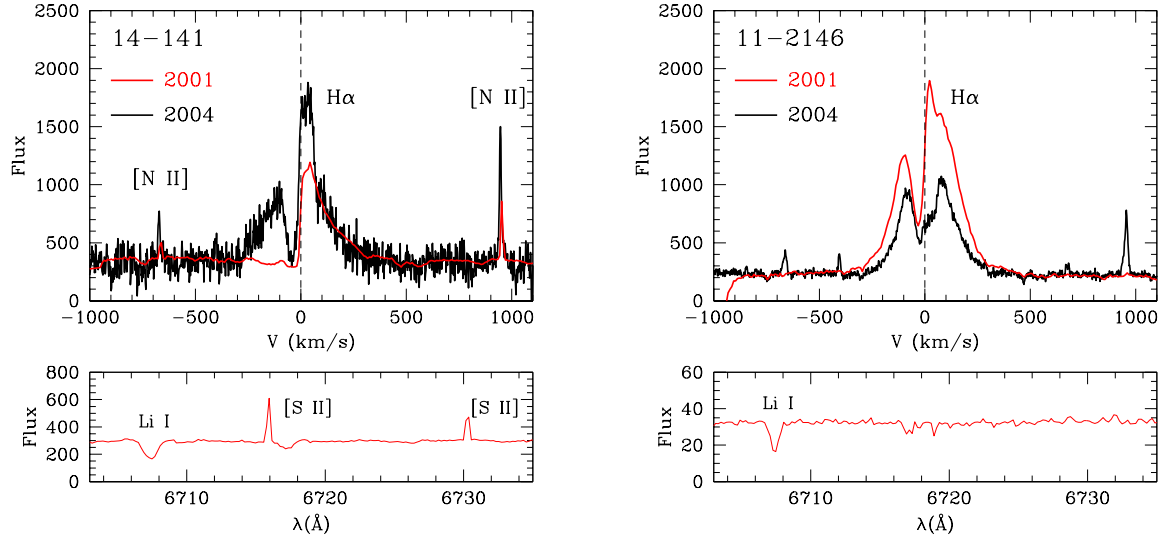


Fig. 5.— H α profile variations of the stars 14-141 and 11-2146. The fluxes are given in arbitrary units, scaled to the continuum levels. Note that the [N II] lines in 11-2146 are due to the undersubtracted nebular emission in the multifiber spectrograph Hectospec, and not related to the object.

Table 1. Observation Summary

Date	Instrument/Telescope	Pointing and Filters	Seeing
2007 June 09	LAICA/3.5 m	Tr 37-1(UVRI)	1.2-1.3"
2007 June 10	LAICA/3.5 m	Tr 37-2(UVRI), Tr 37-3(U)	0.8-1.0"
2007 June 11	LAICA/3.5 m	Tr 37-3(VRI), Tr 37-4(UVRI)	0.6-0.8"
2007 October 5	70 cm KING	NGC 7160 (UVRI)	2"

Note. — Summary of the UVRI observations. Pointing 2 and U band of pointing 3 were taken within less than 2 hours time difference. VRI data for pointing 3 and pointing 4 were also taken within less than 2 hours difference.

Table 2. Optical Data

Name	2MASS ID	Sp. Type	Pointing	U	V	R _J	I _J	A _V	Notes
Tr 37									
72-489	21351481+5721232	K5.0	4c	20.826±0.081	18.159±0.006	16.790±0.022	15.497±0.004	1.76±0.26	n(2'') ^a
72-1427	21351627+5728222	M1.0	3c,4c	20.176±0.046	18.272±0.007	16.618±0.022	15.161±0.004	1.14±0.16	n(4'') ^a
81-541	21351745+5748223	K5.5	4b*	20.511±0.062	17.605±0.015	16.086±0.011	14.598±0.005	2.25±0.29	
72-875	21354975+5724041	M0.5	4c	20.814±0.075	18.245±0.007	16.590±0.022	15.006±0.003	1.51±0.27	SB1:,n(2.5'')
21362507	21362507+5727502	M0.0	4c	21.833±0.188	20.426±0.037	18.578±0.025	—	2.28±0.25	var, SB1
14-141	21364941+5731220	K6.0	2b	19.219±0.083	16.036±0.002	14.508±0.030	13.094±0.003	2.04±0.24	
11-2146	21365767+5727331	K6.0	4c	18.684±0.014	16.662±0.004	15.211±0.022	13.999±0.002	1.62±0.13	n(2''+2'') ^a
11-1209	21365850+5723257	K6.0	4c	17.755±0.010	15.340±0.003	14.040±0.022	13.094±0.002	0.92±0.09	n(4'')
11-1659	21370088+5725224	K5.0	4c	20.155±0.042	17.046±0.004	15.625±0.022	14.534±0.003	1.72±0.09	
11-1499	21370140+5724458	M1.5	4c	21.062±0.094	17.854±0.005	16.185±0.022	14.424±0.003	1.26±0.40	var,n(5'')
11-2322	21370191+5728222	M1.0	4c	18.858±0.016	—	15.357±0.022	13.953±0.002	1.30±0.23	var,n(2'') ^a
14-222	21370607+5732015	K7.0	1a	18.926±0.059	15.801±0.004	14.494±0.011	13.257±0.003	0.90±0.28	
"	21370607+5732015	K7.0	2b	18.828±0.082	15.847±0.002	14.404±0.030	13.140±0.003	1.33±0.20	
14-287	21370649+5732316	M0.0	1a	18.858±0.056	17.095±0.003	15.780±0.004	14.385±0.004	1.11±0.25	var
"	21370649+5732316	M0.0	2b	19.118±0.082	17.258±0.008	15.763±0.030	14.361±0.003	1.11±0.28	var
11-2037	21370703+5727007	K4.5	3c	18.871±0.010	—	—	13.687±0.002	1.63±0.45	
11-1067	21370843+5722484	M0.5	3c	21.635±0.083	17.860±0.017	16.361±0.012	—	0.64±0.12	
14-11	21371031+5730189	M1.5	4a	20.899±0.259	17.653±0.004	16.170±0.005	14.269±0.003	0.85±0.72	
14-125	21371054+5731124	K5.0	2b	19.163±0.082	16.616±0.003	15.224±0.030	14.041±0.003	1.72±0.16	
"	21371054+5731124	K5.0	3c,2b	19.896±0.019	16.616±0.003	15.224±0.030	14.041±0.003	1.72±0.16	
11-1513	21371183+5724486	K7.5	3c	20.988±0.047	17.068±0.016	15.595±0.012	14.191±0.002	1.31±0.27	
11-2131	21371215+5727262	K6.5	3c	20.850±0.041	—	15.853±0.012	14.605±0.003	1.87±0.23	var
11-2031	21371591+5726591	K2.0	3c	18.328±0.006	—	14.240±0.012	13.345±0.002	1.53±0.09	
14-103	21371976+5731043	K7.0	1a	21.856±0.623	18.145±0.005	16.769±0.006	15.350±0.007	1.28±0.38	
14-197	21372368+5731538	K5.5	1a	19.544±0.085	16.864±0.003	15.583±0.011	14.452±0.004	1.20±0.19	SB1:
11-581	21372828+5720326	G9.0	3c	20.508±0.030	16.697±0.016	15.316±0.012	14.159±0.002	3.19±0.09	
14-1017	21372894+5736042	M0.0	3c,1a	20.719±0.039	18.399±0.005	16.874±0.006	15.226±0.006	1.44±0.45	
"	21372894+5736042	M0.0	1a	21.051±0.296	18.399±0.005	16.874±0.006	15.226±0.006	1.44±0.45	
14-335	21372915+5732534	K6.5	1a	21.054±0.313	17.542±0.004	16.100±0.005	14.657±0.005	1.66±0.33	n(4'')
83-343	21373696+5755149	M0.5	2b	21.040±0.123	17.056±0.009	15.455±0.008	14.077±0.003	1.16±0.12	n(5'')
14-183	21373849+5731408	K6.0	1a	19.838±0.105	17.112±0.003	15.648±0.012	14.431±0.004	1.67±0.10	n(4''), SB1:
14-2148	21374184+5740400	M1.5	1a	20.993±0.304	18.260±0.005	16.731±0.006	15.162±0.006	0.67±0.35	
11-1384	21374486+5724135	K6.5	3c	20.630±0.035	17.061±0.016	15.680±0.012	14.388±0.002	1.33±0.26	n(5''+5'')
13-924	21375018+5733404	K5.0	1a	20.582±0.197	17.125±0.003	15.788±0.004	14.472±0.004	1.69±0.30	

Table 2—Continued

Name	2MASS ID	Sp. Type	Pointing	U	V	R _J	I _J	A _V	Notes
12-1984	21375022+5725487	K6.0	3c	20.008±0.020	—	15.561±0.012	14.372±0.002	0.88±0.05	
12-2519	21375107+5727502	K5.5	3c	21.266±0.057	—	15.958±0.012	14.763±0.003	1.93±0.17	
12-1968	21375487+5726424	K6.0	3c	20.257±0.025	—	15.556±0.012	14.396±0.003	1.69±0.26	SB2:
12-1422	21375756+5724197	M0.0	3c	22.215±0.139	18.907±0.019	17.312±0.013	15.621±0.004	1.68±0.43	
12-1091	21375762+5722476	K2.0	3c	19.710±0.015	16.274±0.016	14.984±0.012	13.984±0.002	2.33±0.12	
13-269	21375812+5731199	K6.5	1a	19.666±0.089	16.658±0.005	15.332±0.004	13.988±0.004	1.22±0.35	
12-583	21375827+5720354	M0.0	3c	21.241±0.059	17.650±0.016	16.093±0.012	14.472±0.003	1.50±0.40	n(5")
13-1238	21375926+5736162	M1.0	1a	19.259±0.070	17.902±0.004	16.337±0.006	14.601±0.004	1.15±0.49	
12-2373	21380058+5728253	M1.0	3c	21.776±0.092	—	16.214±0.012	14.759±0.003	1.49±0.18	var
82-272	21380350+5741349	G9.0	1a	19.414±0.080	16.616±0.005	15.266±0.011	14.019±0.004	3.01±0.06	var, SB2
12-1081	21380593+5722438	M0.5	3c	21.989±0.114	18.308±0.017	16.836±0.012	15.438±0.004	0.79±0.28	
13-1161	21380772+5735532	M0.0	1a	20.845±0.241	17.974±0.004	16.515±0.006	15.091±0.004	1.02±0.31	
12-1613	21380848+5725118	M1.0	3c	22.129±0.123	18.326±0.017	16.727±0.012	15.185±0.004	1.06±0.28	
13-1426	21380856+5737076	M0.0	1a	19.858±0.103	19.174±0.009	17.599±0.013	15.748±0.005	1.78±0.60	
13-669	21380928+5733262	K1.0	1a	18.231±0.046	15.834±0.004	14.630±0.011	13.507±0.004	2.17±0.12	
13-350	21381384+5731414	M1.0	1a	21.078±0.304	18.463±0.006	16.880±0.014	15.470±0.005	0.89±0.17	n(3")
54-1781	21381612+5719357	M1.0	3c	21.026±0.045	18.564±0.018	16.922±0.012	15.120±0.003	1.44±0.47	
13-1877	21381703+5739265	K7.0	1a	18.883±0.057	17.189±0.004	15.620±0.004	14.222±0.004	1.84±0.16	
13-277	21381731+5731220	G8.0	1a	15.016±0.040	13.146±0.004	12.090±0.011	11.117±0.003	1.95±0.09	GM Cep, var, SB1:
12-1009	21381750+5722308	K5.5	3c	20.088±0.023	16.689±0.016	15.373±0.012	14.235±0.003	1.31±0.18	var,n(4"+4")
13-819	21382596+5734093	K5.5	1a	19.128±0.065	16.423±0.003	15.173±0.004	14.008±0.004	1.14±0.25	
12-1955	21382692+5726385	K6.5	3c	21.015±0.046	17.388±0.009	16.020±0.012	—	1.04±0.09	
13-236	21382742+5731081	K2.0	1a	17.665±0.042	15.546±0.004	14.431±0.011	13.412±0.004	1.63±0.13	
13-157	21382804+5730464	K5.5	3c	18.588±0.008	16.768±0.016	15.320±0.012	14.012±0.004	1.86±0.20	var,n(4")
13-232	21382834+5731072	M0.0	1a	21.118±0.310	17.428±0.004	16.087±0.006	14.657±0.004	0.68±0.44	
21383216	21383216+5726359	M0.0	3c	21.598±0.076	19.911±0.015	18.202±0.016	16.287±0.007	2.24±0.52	
13-566	21383481+5732500	K5.5	1a	20.977±0.279	18.030±0.004	16.555±0.006	14.959±0.005	2.22±0.43	
13-1709	21384038+5738374	K5.5	1a	20.832±0.251	16.878±0.003	15.591±0.011	14.381±0.003	1.29±0.26	
54-1613	21384332+5718359	K5.0	3c	20.014±0.020	—	15.195±0.012	14.277±0.002	1.06±0.09	
21384350	21384350+5727270	M2.0	3c	24.093±0.775	19.918±0.013	—	—	1.67±0.45	var
54-1547	21384446+5718091	K5.5	3c	19.168±0.010	16.571±0.007	15.321±0.012	14.396±0.003	0.91±0.06	
"	21384446+5718091	K5.5	4d	18.539±0.027	16.571±0.007	15.299±0.011	14.437±0.007	0.91±0.08	
12-2363	21384544+5728230	M0.5	3c	21.420±0.077	17.552±0.009	—	—	1.88±0.45	n(2"), SB1:
12-595	21384622+5720380	K7.0	3c	22.047±0.118	19.512±0.011	17.497±0.013	16.144±0.006	3.12±0.36	var,n(4")
12-1423	21384707+5724207	K7.0	3c	20.814±0.039	17.042±0.016	15.601±0.012	14.382±0.002	1.28±0.14	

Table 2—Continued

Name	2MASS ID	Sp. Type	Pointing	U	V	R _J	I _J	A _V	Notes
12-1010	21385029+5722283	M2.0	3c	20.896±0.039	18.554±0.009	17.043±0.012	15.463±0.004	0.41±0.37	
12-2098	21385253+5727184	M2.5	3c	22.178±0.152	18.775±0.010	—	—	0.98±0.45	
91-506	21385807+5743343	K6.5	4a*	19.777±0.063	17.141±0.013	15.732±0.017	14.546±0.004	1.32±0.15	
12-1617	21390468+5725128	M1.0	4d	20.831±0.089	18.039±0.008	—	—	1.60±0.45	
21-840	21391012+5722323	M1.0	4d	21.201±0.127	18.852±0.011	—	15.647±0.008	1.45±0.04	
13-1048	21391088+5735181	M0.0	2a	19.754±0.039	17.081±0.012	—	14.523±0.003	0.71±0.03	var
13-1250	21391213+5736164	K4.5	2a	18.403±0.018	15.956±0.012	—	13.668±0.003	1.42±0.03	
21-563	21391288+5721088	M1.0	4d	20.807±0.085	17.501±0.008	—	—	1.25±0.45	
24-542	21392957+5733417	K4.0	2a	18.548±0.018	15.986±0.012	14.675±0.032	13.718±0.003	1.53±0.14	
24-515	21393407+5733316	M0.5	2a	19.908±0.043	17.941±0.012	16.396±0.032	15.123±0.004	0.89±0.15	
21-998	21393480+5723277	K5.5	4d	19.798±0.040	17.668±0.008	—	14.961±0.007	1.95±0.03	SB1:
21-33	21393561+5718220	M0.0	4d	20.814±0.075	18.723±0.011	17.138±0.011	15.722±0.008	1.39±0.18	
24-48	21393805+5730439	M0.5	2a	21.972±0.279	17.996±0.012	—	—	1.50±0.45	
21-230	21394169+5719274	M0.5	4d	21.044±0.103	17.922±0.008	—	15.234±0.007	0.71±0.03	
21-1536	21394570+5726242	M0.0	4d	20.636±0.078	19.048±0.013	—	—	1.77±0.45	
52-1649	21394643+5705072	K5.0	2d*	20.051±0.035	17.264±0.007	15.985±0.007	15.043±0.006	1.16±0.04	
21-2251	21394754+5725210	M2.0	4d	21.175±0.115	18.020±0.008	—	—	1.50±0.45	SB1
21-1586	21394793+5726427	K7.0	4d	21.509±0.156	18.402±0.009	—	—	1.49±0.45	
53-1762	21395029+5719177	M0.0	4d	21.391±0.141	18.453±0.009	—	15.655±0.008	1.17±0.03	var, SB1:
21-1692	21400128+5727184	M1.0	4d	21.645±0.170	18.239±0.009	—	15.386±0.007	0.77±0.03	
21-763	21400259+5722090	M0.0	4d	20.511±0.067	17.456±0.008	—	14.950±0.007	0.61±0.03	n(5")
21-895a	21400321+5722505	K5.0	4d	18.983±0.028 ^b	16.640±0.007	—	14.305±0.007	1.37±0.03	n(2") ^b
21400451	21400451+5728363	K5.0	2a	18.045±0.018	16.165±0.012	—	13.893±0.003	1.25±0.03	n(5"+5")
"	21400451+5728363	K5.0	4d	18.215±0.024	16.304±0.007	—	14.088±0.007	1.14±0.03	n(5"+5")
21-1762	21400924+5727393	K5.0	4d	19.753±0.039	16.955±0.007	—	14.519±0.007	1.57±0.03	
24-1736	21401134+5739518	M1.0	2a	19.886±0.045	18.762±0.013	17.138±0.032	15.497±0.004	1.23±0.36	
24-1796	21401182+5740121	K7.0	2a	18.389±0.018	17.341±0.012	15.897±0.032	14.825±0.004	1.15±0.14	SB2:
21-2006	21401390+5728481	K5.0	2a	19.564±0.034	16.933±0.012	15.517±0.032	14.589±0.004	1.55±0.21	
"	21401390+5728481	K5.0	4d	19.457±0.033	16.926±0.007	15.517±0.032	14.707±0.007	1.42±0.30	
22-2651	21402130+5726579	M1.5	4d	18.825±0.026	17.878±0.008	—	15.375±0.007	1.67±0.45 ^c	var
22-1418	21402287+5727329	M1.5	4d	20.799±0.082	17.861±0.008	—	—	0.73±0.45	
23-405	21403134+5733417	K5.0	2a	19.142±0.025	16.610±0.012	15.209±0.032	14.271±0.003	1.52±0.19	
23-570	21403574+5734550	K6.0	2a	18.391±0.017	16.718±0.012	15.276±0.032	14.308±0.003	1.36±0.19	

NGC 7160

Table 2—Continued

Name	2MASS ID	Sp. Type	Pointing	U	V	R _J	I _J	A _V	Notes
01-580	21533707+6228469	K4.5	—	18.38±0.15	17.392±0.042	15.755±0.020	14.737±0.015	2.46±0.40	

Note. — Optical data and 2MASS IDs for the studied stars. Due to the small field overlap, some stars were observed more than once. The pointing and LAICA CCD ID (a,b,c,d) are indicated to show whether all the UVRI measurements were simultaneous (see Table 1). Two pointings are indicated (e.g. 3c+2b), when the U magnitude was observed with pointing 3c, and the VRI data comes from pointing 2. Notes: "var" = variability ($\Delta V > 0.5$ mags) observed, "n(x)" = nearby star at x" projected distance, usually the photometry is not affected. If the nearby star is bright and may affect the photometry, ^a is added (e.g., n(2")^a). Objects that appeared merged with other stars/artifacts are excluded from this study. ^b 21-895b is probably not a member and not a physical companion of 21-895a because of its position in the color-magnitude diagram. ^c The colors of 22-2651 are probably affected by non-standard variability/anomalous extinction. Therefore, we adopt for this object the cluster average extinction.

Table 3. Accretion and Stellar Properties

Name	H α EW(\AA)	H α profile	Disk	L (L_{\odot})	R (R_{\odot})	Age (Myr)	M (M_{\odot})	\dot{M}_U	\dot{M}_{fin}	Comments
Tr 37										
72-489	(-5.5)	—	—	0.38	1.1	22.9	0.9	$0.04^{+0.03}_{-0.01}$	0.04	
72-1427	-16,(-77)	B	TO	0.36	1.5	3.3	0.5	$0.15^{+0.28}_{-0.07}$	0.15	
81-541	-31,(-60)	B	CTTS	1.07	1.9	3.6	1.0	$0.19^{+0.15}_{-0.06}$	0.19	
72-875	(-21)	N	TO	0.50	1.7	2.6	0.5	$0.11^{+0.23}_{-0.06}$	0.11	SB1:, now accreting
21362507	-78,(-86)	B	CTTS	0.11	0.8	26.0	0.6	$0.09^{+0.16}_{-0.05}$	0.09	SB1, HR
14-141	-15,(-5)	B	CTTS	3.79	3.7	0.8	0.9	$0.62^{+0.57}_{-0.33}$	<2.3	
11-2146	-28,-86,(-33)	B	CTTS	1.37	2.3	2.5	1.0	$0.99^{+0.67}_{-0.37}$	0.99	
11-1209	-6,(-4)	B	CTTS	2.31	2.9	1.4	1.0	$0.56^{+0.35}_{-0.23}$	0.56	
11-1659	(-2)	N	N	0.91	1.7	8.3	1.1	$0.02^{+0.02}_{-0.02}$	0	
11-1499	(-7)	N	N	0.73	2.2	1.4	0.4	$0.00^{+0.12}_{-0.02}$	0	
11-2322	-18,(-23)	B	CTTS	1.37	2.9	0.7	0.5	$1.6^{+2.9}_{-0.8}$	1.6	
14-222	(-5)	N:	TOe8	1.87	2.8	1.1	0.7	$-0.06^{+0.03}_{-0.08}$	<0.04	
"	(-5)	N:	TOe8	2.51	3.3	0.9	0.8	$0.34^{+0.28}_{-0.25}$	<0.85	
14-287	-18,(-35)	B	CTTS	0.61	1.8	2.3	0.5	$0.21^{+0.34}_{-0.11}$	0.21	
"	-18,(-35)	B	CTTS	0.79	2.0	2.0	0.6	$0.46^{+0.73}_{-0.24}$	0.46	
11-2037	-43,(-50)	B	CTTS	1.88	2.3	2.5	1.3	$1.1^{+2.6}_{-0.8}$	<9	HR
11-1067	(-7)	N	N	0.28	1.3	5.4	0.5	$0.00^{+0.02}_{-0.01}$	0	HR
14-11	(-5)	N	TO	0.70	2.1	1.4	0.4	$-0.05^{+0.07}_{-0.03}$	0	
14-125	-14,(-13)	B	CTTS	1.44	2.2	3.0	1.1	$0.34^{+0.26}_{-0.12}$	0.34	
"	-14,(-13)	B	CTTS	1.44	2.2	3.0	1.1	$0.34^{+0.21}_{-0.12}$	0.34	
11-1513	(-5)	N	N	0.97	2.1	2.0	0.6	$0.02^{+0.06}_{-0.03}$	0	
11-2131	(-10)	B	CTTS	0.78	1.8	3.0	0.8	$0.25^{+0.12}_{-0.12}$	0.25	HR
11-2031	-5(-5)	B	CTTS	2.93	2.4	4.5	1.6	$0.27^{+0.23}_{-0.17}$	<1	HR
14-103	(-2)	N	N	0.32	1.2	11.6	0.8	$-0.02^{+0.03}_{-0.02}$	0	
14-197	(-2)	N	TOe8	0.77	1.6	7.2	1.0	$0.03^{+0.04}_{-0.01}$	0/<0.14	SB1
11-581	(-9)	N	N	3.39	2.1	24.2	1.4	$-0.51^{+0.36}_{-0.50}$	0	G-age
14-1017	(-55)	B	CTTS	0.41	1.5	3.5	0.5	$0.29^{+0.41}_{-0.14}$	<1.5	
"	(-55)	B	CTTS	0.41	1.5	3.5	0.5	$0.05^{+0.14}_{-0.03}$	<0.5	
14-335	(-20)	P	CTTS	0.74	1.7	4.7	0.8	$-0.02^{+0.05}_{-0.05}$	<0.14	
83-343	(-3)	P	—	1.01	2.4	1.2	0.5	$-0.12^{+0.05}_{-0.05}$	<0.1	
14-183	-14,(-65)	B	CTTS	0.94	1.9	4.8	1.0	$0.16^{+0.12}_{-0.07}$	0.16	
14-2148	(-2)	N	TOe8	0.29	1.4	3.4	0.4	$0.01^{+0.05}_{-0.01}$	0	
11-1384	(-5)	N	N	0.82	1.8	4.3	0.9	$0.06^{+0.05}_{-0.04}$	0	
13-924	(-4)	N	N	0.95	1.8	5.5	1.0	$-0.08^{+0.04}_{-0.09}$	0	

Table 3—Continued

Name	H α EW(Å)	H α profile	Disk	L (L $_{\odot}$)	R (R $_{\odot}$)	Age (Myr)	M (M $_{\odot}$)	\dot{M}_U	\dot{M}_{fin}	Comments
12-1984	(-5)	N	N	0.99	1.9	2.7	0.9	0.64 ^{+0.31} _{-0.23}	0/0.6	HR
12-2519	(-8)	P	CTTS	0.71	1.6	2.8	0.9	0.07 ^{+0.03} _{-0.03}	0.07	HR
12-1968	-8,(-11)	B	CTTS	0.97	1.9	2.8	0.9	0.34 ^{+0.15} _{-0.13}	0.34	SB2, HR
12-1422	(-17)	N	N:*	0.32	1.3	5.8	0.5	0.05 ^{+0.10} _{-0.03}	<0.24	large hole?
12-1091	-2,(-17)	B	CTTS	2.64	2.3	14.1	1.4	0.08 ^{+0.12} _{-0.07}	<0.4	
13-269	(-7)	P	N	1.12	2.1	2.4	0.8	0.01 ^{+0.04} _{-0.03}	0/<0.1	
12-583	(-7)	N	N	0.85	2.1	1.6	0.5	0.11 ^{+0.25} _{-0.07}	0	
13-1238	-31,(-64)	B	CTTS	0.60	1.9	1.8	0.4	0.6 ^{+1.1} _{-0.3}	0.6	
12-2373	(-6)	N	N	0.65	2.0	1.6	0.5	0.07 ^{+0.21} _{-0.05}	0	HR
82-272	-15,(-13)	B	CTTS	3.03	2.0	12.7	1.5	0.07 ^{+0.27} _{-0.34}	<0.9	SB2, G-age
12-1081	(-4)	N	TO	0.24	1.2	7.2	0.5	0.00 ^{+0.02} _{-0.01}	0	
13-1161	(-1)	N	N	0.39	1.4	4.9	0.6	0.01 ^{+0.06} _{-0.01}	0	
12-1613	(-13)	N	N	0.34	1.4	3.3	0.5	0.01 ^{+0.04} _{-0.01}	0	
13-1426	-40,(-109)	B	CTTS	0.30	1.2	5.6	0.5	0.6 ^{+0.8} _{-0.3}	0.6	
13-669	-18,(-22)	B	CTTS	3.23	2.4	6.3	1.6	0.58 ^{+0.20} _{-0.23}	0.58	
13-350	(-9)	N	TO	0.24	1.2	6.4	0.5	0.02 ^{+0.06} _{-0.01}	0	
54-1781	(-13)	P	TO	0.42	1.6	2.5	0.4	0.3 ^{+0.5} _{-0.1}	0.3	
13-1877	-33,(-68)	B	CTTS	1.16	2.2	2.3	0.8	1.6 ^{+1.2} _{-0.8}	1.6	
13-277	-14,-6,(-10,-19)	B	CTTS	27.75	5.9	1.9	2.6	14 ⁺⁶ ₋₄	14	GM Cep, SB1:
12-1009	(-4)	N	TO:	0.98	1.8	5.0	1.0	0.07 ^{+0.06} _{-0.02}	0.07	
13-819	-6,(-10)	B	TO:*	1.12	2.0	3.2	1.0	0.03 ^{+0.04} _{-0.02}	<0.14	large hole
12-1955	(-2)	N	N	0.41	1.3	9.2	0.9	0.01 ^{+0.01} _{-0.01}	0	
13-236	-56,(-47)	B	CTTS	2.70	2.3	5.4	1.6	0.51 ^{+0.26} _{-0.15}	0.51	
13-157	-20,(-14)	B	CTTS	1.54	2.3	2.4	1.0	4.2 ^{+2.9} _{-1.5}	4.2	
13-232	(-3)	N	N:	0.50	1.6	2.7	0.5	-0.05 ^{+0.02} _{-0.03}	0	
21383216	(-129)	B	CTTS	0.22	1.1	8.4	0.5	0.4 ^{+0.5} _{-0.2}	0.4	
13-566	(-5)	N	TOe8	0.75	1.6	6.3	0.9	0.08 ^{+0.14} _{-0.06}	0	
13-1709	(-3)	N	N	0.85	1.7	5.8	1.0	-0.14 ^{+0.06} _{-0.10}	0	
54-1613	(-1)	N	TO	1.13	1.9	3.5	1.1	0.00 ^{+0.01} _{-0.05}	0	HR
54-1547	-33,(-34)	B	CTTS	0.71	1.6	9.0	1.1	0.21 ^{+0.15} _{-0.08}	0.21	
"	-33,(-34)	B	CTTS	0.69	1.5	9.9	1.1	0.18 ^{+0.13} _{-0.06}	0.18	
21384350	(-23)	N	TO	0.14	1.0	7.0	0.4	0.00 ^{+0.05} _{-0.01}	0	HR
12-2363	(-3)	N	N	0.97	2.3	1.0	0.5	0.2 ^{+0.6} _{-0.2}	0	SB1, HR
12-595	(-17)	N	TO	0.35	1.2	22.9	0.9	0.6 ^{+0.3} _{-0.3}	0	scattering?
12-1423	(-2)	N	N	0.78	1.8	4.2	0.9	0.04 ^{+0.03} _{-0.03}	0	

Table 3—Continued

Name	H α EW(\AA)	H α profile	Disk	L (L_{\odot})	R (R_{\odot})	Age (Myr)	M (M_{\odot})	\dot{M}_U	\dot{M}_{fin}	Comments
12-1010	-23,(-20)	B	CTTS	0.19	1.2	6.0	0.4	$0.04^{+0.07}_{-0.02}$	0.04	
12-2098	(-7)	N	—	0.48	1.9	1.8	0.4	$0.03^{+0.08}_{-0.02}$	0	HR
91-506	-31,(-47)	B	CTTS	0.70	1.7	6.5	0.9	$0.09^{+0.07}_{-0.04}$	0.09	
12-1617	-13,(-30)	B	CTTS	0.67	2.0	1.6	0.5	$0.16^{+0.38}_{-0.09}$	0.16	HR
21-840	(-14)	—	CTTS	0.26	1.3	6.4	0.5	$0.06^{+0.08}_{-0.03}$	0.06	
13-1048	-8,(-7)	B	CTTS	0.57	1.7	4.3	0.7	$0.04^{+0.09}_{-0.03}$	<0.3	
13-1250	-4,(-2)	B	TO	1.71	2.2	3.9	1.3	$0.33^{+0.11}_{-0.10}$	0.33	
21-563	(-2)	N	TO	1.11	2.6	0.8	0.5	$0.02^{+0.19}_{-0.03}$	0	HR
24-542	(-4)	N:	N	1.72	2.1	5.0	1.4	$0.24^{+0.19}_{-0.09}$	0.24	now accreting?
24-515	(-11)	P	TO	0.34	1.4	5.6	0.6	$0.10^{+0.18}_{-0.05}$	0.10	
21-998	(-16)	P	CTTS	0.67	1.5	9.7	1.1	$0.33^{+0.19}_{-0.12}$	0.33	SB1
21-33	-51,(-107)	B	CTTS	0.25	1.2	9.6	0.6	$0.07^{+0.11}_{-0.04}$	0.07	
24-48	(-1)	N	N	0.65	1.9	1.8	0.5	$-0.03^{+0.05}_{-0.02}$	0	HR
21-230	(-3)	N	N	0.28	1.3	7.6	0.6	$0.00^{+0.01}_{-0.01}$	0	
21-1536	(-26)	—	CTTS	0.23	1.1	8.8	0.6	$0.18^{+0.29}_{-0.08}$	0.18	HR
52-1649	(-3)	—	—	0.45	1.2	23.2	0.9	$0.01^{+0.01}_{-0.01}$	0	
21-2251	(-4)	N	N	0.83	2.4	0.9	0.4	$0.07^{+0.26}_{-0.05}$	0	SB1, HR
21-1586	(-16)	N	N	0.30	1.1	12.3	0.8	$0.01^{+0.04}_{-0.01}$	0	HR
53-1762	(-2)	N	N	0.25	1.1	16.1	0.7	$0.01^{+0.03}_{-0.01}$	0	
21-1692	(-5)	N	N	0.25	1.2	6.9	0.5	$-0.004^{+0.006}_{-0.003}$	0	
21-763	(-3)	N	N	0.37	1.4	8.3	0.7	$-0.002^{+0.015}_{-0.003}$	0	
21-895a	(-1)	P	TO:*	0.97	1.8	7.7	1.1	$0.21^{+0.09}_{-0.07}$	0.21	
21400451	(-32)	—	CTTS	1.34	2.1	4.9	1.2	$0.71^{+0.36}_{-0.23}$	0.71	
"	(-32)	—	CTTS	1.07	1.9	6.8	1.2	$0.44^{+0.21}_{-0.14}$	0.44	
21-1762	(-3)	N	N*	0.86	1.7	8.7	1.1	$0.07^{+0.02}_{-0.02}$	0.07/0	large hole?
24-1736	-33,(-61)	B	CTTS	0.27	1.3	4.7	0.4	$0.3^{+0.5}_{-0.1}$	0.3	
24-1796	-73,(-124)	B	TOe8	0.49	1.4	9.5	0.9	$0.6^{+0.4}_{-0.3}$	0.6	SB2:
21-2006	(-2)	—	CTTS	0.81	1.6	11.5	1.1	$0.12^{+0.09}_{-0.05}$	0.12	
"	(-2)	—	CTTS	0.68	1.5	17.6	1.0	$0.13^{+0.09}_{-0.05}$	0.13	4d
22-2651	-48,(-34)	B	CTTS	0.26	1.3	21.2	0.8	$0.05^{+0.08}_{-0.02}$	0.05	scattering?
22-1418	(-2)	B	CTTS	0.88	2.4	0.9	0.4	$0.02^{+0.09}_{-0.02}$	<0.3	HR
23-405	-9,(-14)	B	CTTS	1.06	1.9	8.1	1.2	$0.22^{+0.14}_{-0.08}$	0.22	
23-570	-18,(-47)	B	CTTS	0.92	1.8	6.4	1.1	$0.7^{+0.5}_{-0.3}$	0.7	

Table 3—Continued

Name	H α EW(\AA)	H α profile	Disk	L (L_{\odot})	R (R_{\odot})	Age (Myr)	M (M_{\odot})	\dot{M}_U	\dot{M}_{fin}	Comments
NGC 7160										
01-580	(-96)	—	CTTS	1.01	1.7	11.4	1.2	4_{-2}^{+3}	4	

Note. — Accretion and stellar parameters. The H α EW has been compiled from Sicilia-Aguilar et al. (2005b, 2006b, 2008a). The accretion rates are given in units of $10^{-8} M_{\odot} \text{ yr}^{-1}$. It is negative for emission lines, and the values between parentheses correspond to low-resolution spectroscopy. The H α profile is marked as ‘broad’ (B), ‘probably broad’ (P), and ‘narrow’ (N; Sicilia-Aguilar et al. 2006b). The disk type is classified as ‘CTTS’ for normal classical TTS, ‘TO’ (or ‘TOe8’ if only a small excess at $8\mu\text{m}$ is present) for transition objects, and ‘N’ for objects without a detectable excess. Uncertain values are marked with ‘.’. Objects that have no excess down to $8\mu\text{m}$ and have not been detected at $24\mu\text{m}$, but display some signs of accretion, are marked with * and classified as potential TO with large holes. \dot{M}_U indicates the accretion directly measured from the U band photometry, \dot{M}_{fin} is the final value of the accretion rate after requiring a detection probability $>99\%$ (based on 5000 simulations) and H α (see text). Accretion rates are marked as “0” when the simulated data is consistent with zero and there is no further evidence of accretion (see text). If the photometry is consistent with no accretion, but H α suggest that the object is accreting, we consider it as an upper limit. Whenever the measured U band luminosity was found to be below the expected photospheric luminosity in U (L_U is negative), we mark it as a negative accretion rate (corresponding to the accretion rate resulting from the absolute value of L_U). The errors in the luminosity are typically low (\sim few percent). Radii, masses, and ages are derived from the V vs. V-I diagram (or the HR diagram, see text, marked with HR in the “Comments” column), using the Siess et al. (2000) isochrones. For K and M stars, the typical errors in these quantities are $\sim 10\%$, although the age could be more affected by the presence of unresolved binaries. The age of early K and G-type stars is far more uncertain due to general problems establishing the birthline (Hartmann 2003); such objects are marked as “G-age”. Binary information for spectroscopic binaries (unresolved, similar mass, single-lined [SB1] or double-lined [SB2] spectroscopic binaries) is taken from Sicilia-Aguilar et al. (2006b).

Table 4. Significance of the trends in \dot{M} versus disk structure, age and mass

Trend	r	p	Confidence interval	Comments
\dot{M} vs. $\alpha(\text{H-4.5})$	0.10	0.52	-0.26,0.44	No significant correlation
\dot{M} vs. $\alpha(\text{H-8.0})$	0.21	0.16	-0.15,0.53	No significant correlation
\dot{M} vs. $\alpha(3.6\text{-}5.8)$	0.38	0.02	0.03,0.64	Moderate correlation
\dot{M} vs. $\alpha(5.8\text{-}8.0)$	0.02	0.87	-0.33,0.38	No significant correlation
\dot{M} vs. $\alpha(\text{H-24})$	-0.01	0.97	-0.38,0.37	No significant correlation (survey not complete at $24\mu\text{m}$)
\dot{M} vs. $\alpha(8.0\text{-}24)$	-0.26	0.12	-0.58,0.13	Weak potential anticorrelation (survey not complete at $24\mu\text{m}$)
\dot{M} vs. age (All)	-0.60	<0.001	-0.70,-0.48	Anticorrelation
\dot{M} vs. age (Cep OB2 only)	-0.32	0.03	-0.61,0.04	Moderate anticorrelation
\dot{M} vs. M_*	0.32	0.03	-0.03, 0.59	Moderate correlation

Note. — Spearman’s correlation coefficients (r), probability (p) and confidence intervals of the different trends explored. A value of $r \sim 1$ indicates a perfect positive correlation, $r \sim -1$ indicates anticorrelation, $r \sim 0$ suggests that the two quantities are uncorrelated. The probability that such a correlation coefficient is from a sample of random data is indicated by p.

Table 5. Variable accretion (type II) candidates

ID	$\dot{M}_{02/03}$ ($10^{-8} M_{\odot} \text{ yr}^{-1}$)	\dot{M}_{07} ($10^{-8} M_{\odot} \text{ yr}^{-1}$)	Comments
72-875	<0.001	$0.11^{+0.23}_{-0.06}$	SB1:
14-141	<0.1	<2.3	spectroscopically confirmed
11-2146	16	$1.0^{+0.7}_{-0.3}$	spectroscopically confirmed, type III variable
11-2031	1.6	$0.3^{+0.2}_{-0.2}$	
13-1238	11	$0.6^{+1.1}_{-0.3}$	
82-272	24	<0.9	SB2, uncertain, type III variable
13-277	<30	14^{+6}_{-4}	GM Cep, spectroscopically confirmed
13-236	2	$0.5^{+0.3}_{-0.2}$	
13-1250	0.1	$0.33^{+0.11}_{-0.10}$	TO
21-1762	0.2	$0.07^{+0.02}_{-0.02}$	large hole candidate

Note. — Candidates to have type II variability, related to a variable accretion rate.

Table 6. Variable extinction (type III) candidates

ID	A_V (2001)	A_V (2007)	Comments
11-2146	2.58 mag	1.62 ± 0.13 mag	type II variable
14-287	2.20 mag	1.1 ± 0.3 mag	disk
11-1067	1.20 mag	0.64 ± 0.12 mag	
11-581	1.50 mag	3.19 ± 0.09 mag	
82-272	3.58 mag	3.01 ± 0.06 mag	disk, SB2, type II candidate
12-1955	1.42 mag	0.71 ± 0.09 mag	
12-595	1.18 mag	3.1 ± 0.4 mag	TO, evidence of scattering
21-840	2.15 mag	1.45 ± 0.04 mag	disk
13-1048	1.67 mag	0.71 ± 0.03 mag	disk
21-230	1.50 mag	0.71 ± 0.03 mag	
21-1692	1.68 mag	0.71 ± 0.03 mag	
21-763	1.20 mag	0.61 ± 0.03 mag	
21-1762	1.75 mag	1.57 ± 0.03 mag	

Note. — Candidates to have type III variability, related to a variable extinction, probably caused by circumstellar matter.